Université d'Ottawa · University of Ottawa

Université d'Ottawa · University of Ottawa

FACULTÉ DES ÉTUDES SUPÉRIEURES ET POSTDOCTORALES

FACULTY OF GRADUATE AND POSTDOCTORAL STUDIES

Xiaowen, LIU
AUTEUR DE LA THÈSE - AUTHOR OF THESIS

M. A. Sc. (Electrical Engineering)
GRADE - DEGREE

Faculty og Engineering
FACULTÉ, ÉCOLE, DÉPARTEMENT - FACULTY, SCHOOL, DEPARTMENT

TITRE DE LA THÈSE - TITLE OF THE THESIS

The Use of FDTD Method for Electromagnetic Analysis in the Presence of Time-Varying Media

D.A. Mc Namara
DIRECTEUR DE LA THÈSE - THESIS SUPERVISOR

CO-DIRECTEUR DE LA THÈSE - THESIS CO-SUPERVISOR

EXAMINATEURS DE LA THÈSE - THESIS EXAMINERS

M. Yagoub

Q.J. Zhang

J.-M. De Koninck, Ph.D

LE DOYEN DE LA FACULTÉ DES ÉTUDES SUPÉRIEURES ET POSTDOCTORALES

DEAN OF THE FACULTY OF GRADUATE AND POSTDOCTORAL STUDIES

The Use of the FDTD Method for Electromagnetic Analysis in the Presence of Time-Varying Media

by

Xiaowen Liu

A thesis submitted to the
Faculty of Graduate and Postdoctoral Studies
in partial fulfillment of the requirements for the degree of

Master of Applied Science
in Electrical Engineering

Ottawa-Carleton Institute for Electrical and Computer engineering
School of Information Technology and Engineering
Faculty of Engineering
University of Ottawa

July 2004

Your file Votre référence
ISBN: 0-494-01532-2
Our file Notre référence
ISBN: 0-494-01532-2

ABSTRACT

In this thesis a straightforward means of including independently time-varying material properties in finite-difference time-domain (FDTD) formulations is presented. The approach is systematically applied to three classes of problems, namely electromagnetic wave propagation through a medium with time-varying permittivity, electromagnetic wave propagation along a medium with time-varying permittivity, and electromagnetic wave radiation from a source on a medium with time-varying permittivity. The first-mentioned class of problem has received limited attention in the literature either analytically or numerically. The second and third classes have received virtually no attention in the literature using any approach prior to the present study. By carefully selecting examples from the above-mentioned classes of problem the correctness of the FDTD predictions for these examples has been confirmed in spite of the unavailability of precise analytical solutions (due to the inherent difficulty of finding such solutions for time-invariant problems in electromagnetics) or experimental results (due to the fact that appropriate materials are not yet extant). The computational analysis of the examples from the second and third class of problem, respectively the microstrip line and microstrip patch antenna on substrates with time-varying permittivity, represent the first analysis of any kind to have been reported for such structures. We show how mixed frequencies can be generated by such structures. The geometry of these structures might be further used to emphasise or de-emphasise certain mixed frequencies. The effectiveness of using the FDTD method for devices comprised of time-varying substrates, and how the FDTD results can be processed (eg. using the method of determining the instantaneous frequency that was devised, or using Fourier transforms) to extract a physical understanding of the device behaviour, has been demonstrated. The work completed in this thesis has established the fact that the FDTD is a valid, and in fact perfectly suited, electromagnetic simulation method for future electromagnetic devices which might incorporate independently time-varying materials.

Keywords: Computational Electromagnetics, FDTD, Time-Varying Medium.

ACKNOWLEDGEMENTS

I would like to thank my supervisor Dr. Derek McNamara for his support, guidance and funding during the research and writing of this thesis. The experience and knowledge I gained from him during our work is, and will be, of great value to me throughout my career. I would also like to thank Dr. Pierre Berini for providing partial financial support for my studies.

I owe thanks to my colleagues Ms. Xiangjun Meng, Mr. Wei Fang, Mr. Liguo Yang, Mr. Pradiv Sooriyadevan, Mr. Prasun Sharma, and my husband, parents, family members and friends for always being there for me, and for unselfishly supporting me from the very beginning of my graduate studies.

TABLE OF CONTENTS

GLOSSARY

1-D	One Dimensional
2-D	Two Dimensional
3-D	Three Dimensional
ABC	Absorbing Boundary Condition
ADI	Alternation Direction Implicit
B	Magnetic Flux Density
C	Capacitance
CAD	Computer Aided Design
CEM	Computational Electromagnetics
D	Electric Flux Density
DFT	Discrete Fourier Transform
E	Electric Field
F	Frequency
FDTD	Finite Difference Time Domain
FEM	Finite Element Method
FETD	Finite Element Time Domain
H	Magnetic Field
I	Current
J	Electric Current Density
M	Magnetic Current Density
MoM	Method of Moments
PEC	Perfect Electric Conductor

PML	Perfectly Matched Layer
S	Scattering Parameter
TE	Transverse Electric
TEM	Transverse Electromagnetic
TM	Transverse Magnetic
V	Voltage
Z	Impedance

TABLE OF SYMBOLS AND VARIABLES

Δx	Discretization Size Along the x Axis
Δy	Discretization Size Along the y Axis
Δz	Discretization Size Along the z Axis
maxx	Total Size of Yee Cells Along the x Axis
maxy	Total Size of Yee Cells Along the y Axis
maxz	Total size of Yee Cells Along the z Axis
Δt	Disctrtization Size Along the t Axis
n	Total Time Steps
ε	Permittivity
μ	Permeablility
θ,φ	Polar Coordinates
$\Delta\theta,\Delta\varphi$	Resolution of Discretized Solid Angle

List of Figures

List of Tables

CHAPTER 1
Introduction

1.1 MATERIALS WITH ELECTRONICALLY/PHOTONICALLY CONTROLLABLE PROPERTIES

The electromagnetic properties of a material are described by three parameters, namely permittivity, conductivity and permeability. The technology of materials synthesis is advancing rapidly, and it is not unrealistic to expect that in the future low-loss materials will be available whose permittivity, permeability and/or conductivity will be electronically or optically controllable in a rapid fashion. There have already been several publications (eg. [1,2,3,4]) describing the realisation of controlled components using bulk distributed properties directly rather than semi-lumped active components, albeit for those cases where this control takes place on a time scale that is very much larger than a signal period (i.e. the devices are best described as being electronically reconfigurable).

In this thesis we wish to explore the suitability of the finite-difference time-domain (FDTD) method as a tool for the full-wave electromagnetic modeling of devices composed of materials with independently time-varying properties. By the term "independently time-varying" we mean that the property in question can be altered as a function of time independent of the electromagnetic field values. The material of concern is not a non-linear material but a controllable material. Throughout the thesis we will always assume that the materials being considered are isotropic, linear, and non-dispersive. In other words, while we may control the value of the value of the materials' permittivity (for example) as a function of time, the permittivity does not depend on the field orientation, the magnitude of the electromagnetic fields, or their frequency.

1.2 ELECTROMAGNETIC ANALYSIS IN THE PRESENCE OF INDEPENDENTLY TIME-VARYING MEDIA

Electromagnetic analysis is always based on the mathematical model known as Maxwell's equations [5]. Many computational methods have been developed for the solution of Maxwell's equations, both in the frequency-domain and the time-domain. Time-domain formulations are the most natural ones for electromagnetics problems involving non-linear materials or other non-single-frequency field variations. They will, for similar reasons, be the domain of choice when there are independently time-varying materials present.

There are several time-domain electromagnetic modeling methods. These are the finite-difference time-domain (FDTD) method [6], the transmission line matrix (TLM) method [7], the finite-element time-domain (FETD) method [8,9], and integral equation methods formulated in the time-domain [10].

The FETD method is currently less mature than the FDTD method. Its principal advantage lies in its ability to deal with geometries that do not consist of rectangularly shaped obstacles and materials only. This allows it to use a non-uniform grid. However, the formulation is more complicated. Due to the fact that the problems of interest in this thesis are indeed composed of rectangular shapes we have no special need to use the FETD approach. Furthermore, the FDTD method's maturity means that virtually all issues other than the inclusion of independently time-varying materials have been thoroughly studied, and that we are therefore able to devote all effort on the time-varying material aspects which are the main issues of this thesis. Thus we have selected the FDTD approach before the FETD method.

The TLM method is very similar to the FDTD method, and it is difficult to say (at least with quantitative certainty) which is actually more widely-used in electromagnetic engineering practice. Codes for both these methods are available commercially. The one method does not appear to have any clearcut advantage over the other, and one simply has to make a choice. In this thesis we wished to investigate the use of the FDTD for problems involving independently time-varying problems, and have not considered the TLM method.

The use of integral equation approaches in the time-domain is, compared to all the other methods mentioned above, in its infancy. The formulations are, by their very nature, problem-specific and numerically very complicated compared to the other time-domain methods mentioned.

1.3 OVERVIEW OF THE THESIS

The aim of this thesis is to explore the suitability of the FDTD method as a means for the full-wave electromagnetic modeling of devices composed of materials with independently time-varying properties. One difficulty is that there is very little in the literature with which we can compare computed results. In essence, this is due to the fact that, as indicated earlier in the thesis, the aim is to explore the use of the FDTD method in applications that might arise in the future as increasingly controllable materials (which are not yet available) are developed. Thus we cannot appeal to experimental validation. It was thus necessary to carefully select the problems to be considered so that confidence in the correctness of the computed results could be argued by other means. Three problems were chosen. These are:

- A plane wave incident on a dielectric slab of fixed thickness whose permittivity is independently time-varying. This first problem is considered in Chapter 3, and might be classified as a case of "electromagnetic wave *propagation through* a time-varying medium".

- An electromagnetic wave propagating along a section of microstrip line of fixed width and substrate height, but whose substrate permittivity is independently time-varying. This is the subject of Chapter 4, and might be classified as a case of "electromagnetic wave *propagation along* a time-varying medium".

- The far-zone electromagnetic field of a microstrip patch antenna of fixed dimensions and substrate height, but whose substrate permittivity is independently time-varying. This is discussed in Chapter 5, and might be classified as a case of "electromagnetic wave *radiation from* a time-varying medium".

Chapter 2 briefly expounds the basis of the electromagnetic model and the essentials of the FDTD method, while Chapter 6 provides some general conclusions and suggestions for future work.

1.4 REFERENCES FOR CHAPTER 1

[1] S.J.Fiedziuszko, I.C.Hunter, T.Itoh, Y.Kobayashi, T.Nishikawa, S.N.Stitzer & K.Wakino, "Dielectric materials, devices and circuits", IEEE Trans. Microwave Theory Tech., Vol.50, No.3, pp.706-720.

[2] C.Shin, R.Nevels, F.Strieter & J.R.Baird, "An electronically controlled transmission-line phase shifter", Microwave Opt. Tech. Letters, Vol.40, No.5, pp.402-406, March 2004.

[3] J.D.Arnould, R.Gary & A.Vilcot, "3D photo-induced load modeling for optically controlled microwave microstrip line", Microwave Opt. Tech. Letters, Vol.40, No.5, pp.356-359, March 2004.

[4] S.W.Kichoefer, J.M.Pond, H.S.Newman, W.Kim & J.S.Horwitz, "Ferroelectric-ferrite tunable phase shifters", IEEE Int. Microwave Symposium (IMS) Digest, 2000 (CD-ROM)

[5] E.J.Rothwell & M.J.Cloud, *Electromagnetics* (CRC Press, 2001).

[6] A.Taflove and S.C.Hagness, *Computational Electrodynamics: The Finite-Difference Time-Domain Method, 2nd edition* (Artech House, 2000)

[7] D.G.Swanson & W.J.R.Hoefer, *Microwave Circuit Modelling Using Electromagnetic Fieldsa Simulation* (Artech House, 2003)

[8] J.F.Lee, R.Lee and A.Cangellaris, "Time-Domain Finite-Element Methods", IEEE Transactions on Antennas and Propagation, Vol. 45, No. 3, March 1997.

[9] D.-K.Sun, J.-F.Lee & Z.Cendes, "The transfinite-element time-domain method", IEEE Trans. Microwave Theory Tech., Vol.51, No.10, pp.2097-2105, October 2003.

[10] S.M.Rao (Edit.), *Time Domain Electromagnetics* (Academic Press, 1999)

CHAPTER 2

Electromagnetic Modelling in the Presence of Independently Time-Varying Media

2.1 INTRODUCTION

This chapter will serve three purposes. Firstly, it will in Section 2.2 place the analysis done in this thesis in the context of electromagnetic theory generally. Secondly, it will in Section 2.3 serve to introduce the FDTD method and in Section 2.4 the important issue of sources. Thirdly, it will in Section 2.5 present a review of existing electromagnetic analyses in the presence of independently time-varying media. Section 2.6 will provide some concluding remarks to the chapter.

2.2 THE FUNDAMENTAL ELECTROMAGNETIC MODEL

All classical electromagnetic phenomena are governed by Maxwell's equations, which may be written in differential equation form as [1,2,3,4]

$$\nabla \cdot \vec{D} = \rho \tag{2-1}$$

$$\nabla \cdot \vec{B} = 0 \tag{2-2}$$

$$\nabla \times \vec{E} = -\frac{\partial \vec{B}}{\partial t} \tag{2-3}$$

$$\nabla \times \vec{H} = \vec{J} + \frac{\partial \vec{D}}{\partial t} \tag{2-4}$$

The term $\overline{J}$ consists of both impressed electric current density sources $\overline{J}_{source}$ and any response current densities that exist as a result of the fields (eg. a conduction current density $\overline{J}_c$). In isotropic non-dispersive materials (the type we will be considering in thesis, as mentioned in Section 1.1) the so-called constitutive relations [1]

$$\overline{D} = \varepsilon \, \overline{E} \tag{2-5}$$

$$\overline{B} = \mu \, \overline{H} \tag{2-6}$$

$$\overline{J}_c = \sigma \, \overline{E} \tag{2-7}$$

relate the field vectors shown to one another. In the above expressions ε is the material permittivity, μ the permeability, and σ the conductivity. We will often refer to ε, μ and σ as the "electromagnetic properties" of the material.

At points on the interface between materials of different electromagnetic properties one or more of the field vectors may have discontinuous components, and hence one or more of the above differential equation forms may not apply. At such points the field behaviour is described by the boundary conditions [1] :

$$\begin{aligned} &\hat{n}\times(\vec{E}_1 - \vec{E}_2) = 0 \qquad && \hat{n}\cdot(\vec{D}_1 - \vec{D}_2) = \rho_s \\ &\hat{n}\times(\vec{H}_1 - \vec{H}_2) = \vec{J}_s \qquad && \hat{n}\cdot(\vec{B}_1 - \vec{B}_2) = 0 \end{aligned} \tag{2-8}$$

These boundary conditions are derivable (as are the differential equation forms) from the integral forms of Maxwell's equations [1]. In (2-8) the vector $\hat{n}$ is normal to the interface between the two material regions (and points from material#2 to material#1), $\overline{J_s}$ is an electric surface current density on the interface, and ρ_s an associated electric surface charge density.

A homogeneous medium (or material) is one in which the electromagnetic properties are uniform everywhere in the region of interest. In an inhomogeneous medium these properties are a function of position (that is, their values are functions of the spatial variables). In an isotropic material, the electromagnetic properties do not depend on the orientation of the electromagnetic field vectors, and thus the ε, μ and σ are scalar quantities. This is not the case in an anisotropic medium. In this thesis all materials are considered isotropic. In linear materials the values of ε, μ and σ do not depend on the strength of the field vectors. In nonlinear materials one they do depend on $|\overline{E}|$ and/or $|\overline{H}|$. A time-invariant medium is one whose electromagnetic properties do no change with time. In an *independently time-varying* one may have $\varepsilon(t)$, $\mu(t)$ and/or $\sigma(t)$, their variation with respect to time t being independent of the values of the field vectors. Materials in which the material constants are functions of frequency, namely $\varepsilon(\omega)$, $\mu(\omega)$ or $\sigma(\omega)$, are called dispersive materials; in such cases it is not possible to write the constitutive relations in the simple form (2-5) through (2-7), the relationship becoming one involving convolution integrals with respect to time. In this thesis all materials are assumed to be non-dispersive. Finally, although the methods considered will apply to magnetic materials as well, we will consider only non-magnetic materials (that is, those which have $\mu = \mu_0$).

2.3 OVERVIEW OF THE THREE-DIMENSIONAL *FDTD* ALGORITHM

2.3.1 Preliminary Remarks

The finite-difference time-domain (FDTD) method [4,5] is a good choice for the applications this thesis has in mind. It is a numerical method that directly solves the full-wave vector form of Maxwell's equations in the time domain. It has been applied to many different classes of problem. The inherent flexibility stemming from the fact that it is a differential equation based method allows it to deal with quite arbitrary rectangular geometries and material inhomogeneities. Although the treatment of dispersive materials is perhaps less complicated using frequency domain methods, means of incorporating such dispersion in the FDTD approach are by now well-developed. Being a time-domain method it is well-suited to problems involving non-linear materials. It is for similar reasons that we consider it applicable to the case where independently-time-varying materials are present, and thus use it as the only electromagnetic simulation tool in this thesis.

The theory and applications of the FDTD method are described in great detail in textbooks (eg. [5]), albeit not for problems involving indepently time-varying materials. The purpose of this section is therefore not to provide a complete treatment of the method but rather to simply emphasise and discuss those aspects that are particularly important to its application in this thesis.

2.3.2 Outline of the Manner in which the FDTD Method is Introduced

In Section 1.3 we provided motivation for the choice of problems selected for consideration in Chapters 3 through 5. In Chapter 3 we will require a one-dimensional FDTD formulation, whereas in Chapters 4 and 5 a fully three-dimensional formulation will be needed. We will in this section provide a general overview of the three-dimensional FDTD formulation. Then, in Chapter 3, we will simplify this to the one-dimensional form required there. Although this might at first appear to be the "wrong way round" of approaching the matter, it turns out that it simplifies things. In Chapters 4 and 5 we will discuss some additional three-dimensional FDTD formulation issues related to the specific problems considered.

2.3.3 The Essential FDTD Algorithm (Updating Equations)

The FDTD algorithm is used to solve the time dependent Maxwell's curl equations using second-order accurate central difference approximations to sample the continuous electromagnetic fields in space and time steps. The algorithm staggers the electric and magnetic fields in both time and space, using the one to compute the other as time progresses using a so-called updating equation, and for this reason is often referred to as a leap-frog algorithm. In the case of non-dispersive materials we can use the constitutive relations to rewrite Maxwell's curl equations as

$$\begin{aligned}\nabla\times\vec{E} &= -\mu\frac{\partial\vec{H}}{\partial t}\\ \nabla\times\vec{H} &= \frac{\partial\{\varepsilon\vec{E}\}}{\partial t}-\sigma\vec{E}+\vec{J}^{source}\end{aligned} \qquad (2\text{-}9)$$

In a rectangular coordinate system equations (2-9) can be written as six scalar partial differential equations

$$\begin{aligned}\frac{\partial H_x}{\partial t} &= \frac{1}{\mu}\left(\frac{\partial E_y}{\partial z}-\frac{\partial E_z}{\partial y}\right)\\ \frac{\partial H_y}{\partial t} &= \frac{1}{\mu}\left(\frac{\partial E_z}{\partial x}-\frac{\partial E_x}{\partial z}\right)\\ \frac{\partial H_z}{\partial t} &= \frac{1}{\mu}\left(\frac{\partial E_x}{\partial y}-\frac{\partial E_y}{\partial x}\right)\end{aligned} \qquad (2\text{-}10)$$

$$\frac{\partial \varepsilon E_x}{\partial t} = \frac{\partial H_z}{\partial y} - \frac{\partial H_y}{\partial z} - \sigma E_x + J_x^{source}$$
$$\frac{\partial \varepsilon E_y}{\partial t} = \frac{\partial H_x}{\partial y} - \frac{\partial H_z}{\partial x} - \sigma E_y + J_y^{source} \qquad (2\text{-}11)$$
$$\frac{\partial \varepsilon E_z}{\partial t} = \frac{\partial H_y}{\partial x} - \frac{\partial H_x}{\partial y} - \sigma E_z + J_z^{source}$$

In order to discretize the problem, the region in which the field exists is divided into electrically small rectangular cells ("Yee cells"). Figure 2.1 illustrates the spatial positions of the electric and magnetic field components within each Yee cell of the FDTD lattice. The three electric field components are computed at the midpoints of the edges of the cell, while the three magnetic field components are computed at the midpoints of the faces of the same cell.

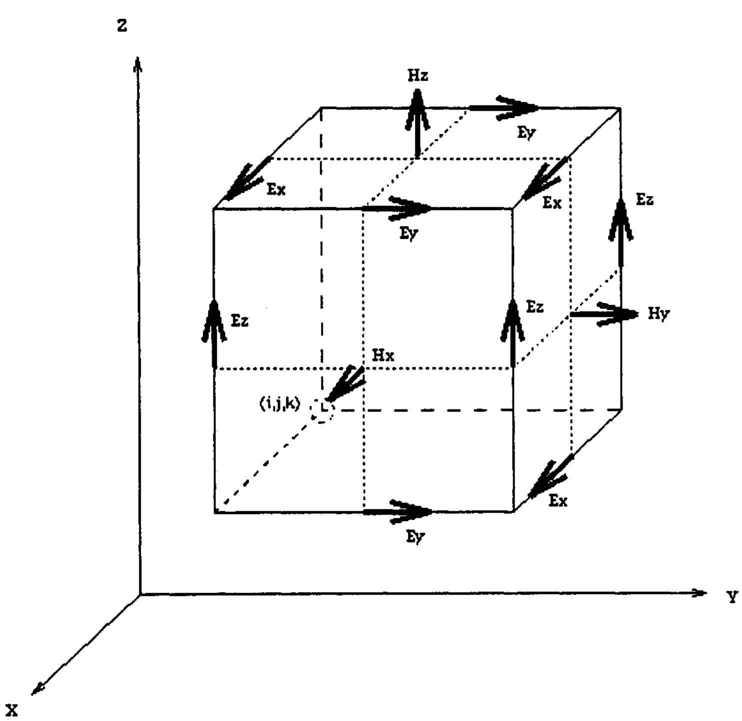

Figure 2.1 : Standard Yee Cell (After [5])

The FDTD algorithm approximates the derivatives in the six differential equations using finite differences, and obtains the updating equations for the six field components as

$$H_x^{n+\frac{1}{2}}(i,j,k) = H_x^{n-\frac{1}{2}}(i,j,k) - \frac{\Delta t}{\mu_o}\left[\frac{E_z^n(i,j,k) - E_z^n(i,j-1,k)}{\Delta y} - \frac{E_y^n(i,j,k) - E_y^n(i,j,k-1)}{\Delta z}\right]$$

$$H_y^{n+\frac{1}{2}}(i,j,k) = H_y^{n-\frac{1}{2}}(i,j,k) - \frac{\Delta t}{\mu_o}\left[\frac{E_x^n(i,j,k) - E_x^n(i,j-1,k-1)}{\Delta z} - \frac{E_z^n(i,j,k) - E_z^n(i-1,j,k)}{\Delta x}\right]$$

$$H_z^{n+\frac{1}{2}}(i,j,k) = H_z^{n-\frac{1}{2}}(i,j,k) - \frac{\Delta t}{\mu_o}\left[\frac{E_y^n(i,j,k) - E_y^n(i-1,j,k)}{\Delta x} - \frac{E_x^n(i,j,k) - E_x^n(i,j-1,k)}{\Delta y}\right]$$

$$\begin{aligned} E_x^{n+1}(i,j,k) &= \frac{\varepsilon^n(i,j,k)}{\varepsilon^{n+1}(i,j,k)} E_x^n(i,j,k) \\ &+ \frac{\Delta t}{\varepsilon^{n+1}(i,j,k)}\left[\frac{H_z^{n+\frac{1}{2}}(i,j+1,k) - H_z^{n+\frac{1}{2}}(i,j,k)}{\Delta y} - \frac{H_y^{n+\frac{1}{2}}(i,j,k+1) - H_y^{n+\frac{1}{2}}(i,j,k)}{\Delta z}\right] \end{aligned} \tag{2-12}$$

$$\begin{aligned} E_y^{n+1}(i,j,k) &= \frac{\varepsilon^n(i,j,k)}{\varepsilon^{n+1}(i,j,k)} E_x^n(i,j,k) \\ &+ \frac{\Delta t}{\varepsilon^{n+1}(i,j,k)}\left[\frac{H_x^{n+\frac{1}{2}}(i,j,k+1) - H_z^{n+\frac{1}{2}}(i,j,k)}{\Delta z} - \frac{H_y^{n+\frac{1}{2}}(i+1,j,k) - H_y^{n+\frac{1}{2}}(i,j,k)}{\Delta x}\right] \end{aligned}$$

$$E_z^{n+1}(i,j,k) = \frac{\varepsilon^n(i,j,k)}{\varepsilon^{n+1}(i,j,k)} E_z^n(i,j,k)$$

$$+ \frac{\Delta t}{\varepsilon^{n+1}(i,j,k)} \left[\frac{H_y^{n+\frac{1}{2}}(i+1,j,k) - H_y^{n+\frac{1}{2}}(i,j,k)}{\Delta x} - \frac{H_x^{n+\frac{1}{2}}(i,j+1,k) - H_x^{n+\frac{1}{2}}(i,j,k)}{\Delta y} \right]$$

The (i,j,k) denote spatial points in the cell, while the superscripts in terms of n denote points in time. We will in this thesis be considering materials which have zero conductivity and whose permeability is that of free space. Only the permittivity will be allowed to vary either in space or in time. The above updating equations have assumed this implicitly.

2.3.4 Stability Issues

The electric and magnetic field components are computed at different times. The time difference is $\Delta t/2$, where Δt is the time step. The quantities $\Delta x, \Delta y, \Delta z$ are the cell dimensions along the x,y,z axes. If values of Δx, Δy or Δz are too large, the algorithm may not calculate the wave propagation with sufficient accuracy, and the simulation will fail. The choice of Δx, Δy or Δz is related to the value chosen for Δt. If the Δt value chosen for the model is too large, the algorithm cannot correctly determine the locations of all waves in a specific time in the future. In order to ensure numerical stability the Δx, Δy and Δz, and the Δt, must be chosen so that the Courant stability criterion [5]

$$\Delta t \leq \frac{1}{c \cdot \sqrt{(\frac{1}{\Delta x})^2 + (\frac{1}{\Delta y})^2 + (\frac{1}{\Delta z})^2}} \tag{2-13}$$

is satisfied.

2.3.5 The FDTD Implementation of Boundary Conditions

A. Boundary Conditions at Perfectly Conducting Surfaces

At points on a perfect electrically conducting surface the tangential component of **E** is zero, and the FDTD updating equation changes for such points, consisting of the setting of certain components to zero. For example, if the top surface of the Yee cell in Figure 2.1 is tangential to a perfect conductor then the FDTD updating equation becomes

$$E_y(i,j,k-1) = E_y(i,j,k) = E_z(i,j-1,k) = E_z(i,j,k) = H_x(i,j,k) = 0 \qquad (2\text{-}14)$$

B. Boundary Conditions at Points on the Interface Between Materials of Different Permittivities

At points that lie on the interface between different dielectric materials (of permittivities ε_1 and ε_2 say) the permittivity is actually not uniquely defined, and a problem arises as to which of the two permittivities should be used in the updating equations at such points. Usually [5] the average value of the two permittivities is used, namely $(\varepsilon_1 + \varepsilon_2)/2$, and is sometimes loosely referred to as "media averaging".

C. Absorbing Boundary Conditions

Absorbing boundary conditions (ABCs) are sued to truncate the solution region over which the FDTD is applied in such a way that the FDTD method is "not aware" that this truncation has been done. Mur's first and second order ABCs [5] are used in this thesis. In the one-dimensional code to be used in Chapter 3 we will use the first-order ABC. In the three-dimensional code to be used in Chapters 4 and 5 the second-order ABC is applied. The FDTD implements these ABCs by providing special updating equations for points lying on the truncation boundary on which the ABC is enforced. These update equations are described in Appendix I.

2.4 SOURCE TYPES, AND THE TIME-DEPENDENCE OF SOURCES & MATERIAL PROPERTIES

2.4.1 Hard Versus Soft Sources : Requirements for the FDTD Modelling of Time-Varying Materials

A source is called *hard* if the total field at a source point is forced to have specified impressed values, irrespective of what is going on around it. A hard source is usually set up by simply by assigning a desired time function to the total electric field at specific points in the FDTD spatial grid. It is independent of the fields at neighbouring points. A *soft* source is one that does not impress the value of the total electric field at any point. It can be implemented in many ways. In the analysis to be discussed in this thesis the generation of frequency components other than that of the input signal is expected. Thus we cannot use a hard source at any point, since this would artificially force the field to have specific frequency components (that is, its spectrum would be forced to be the same as that of the source).

2.4.2 The Time-Dependence of Sources

Irrespective of whether a hard or soft source is used the specific time-variation of the chosen source must be selected. In many cases where the FDTD method is used one desires to exploit one of its definite advantages over frequency-domain methods – namely the ability to so specify the time-variation of the source that a single simulation provides the system response over a band of frequencies rather than a single frequency. Thus baseband Gaussian pulse or sinusoidally modulated Gaussian pulse waveforms are often used [6].

Normally a sinusoidal excitation would be appropriate when just a single frequency is of interest. However, in the case of independently time-varying materials, we are also interested in an excitation that is essentially a single frequency sinusoid. This enables one to properly keep track of any additional frequencies that are generated due to the varying material properties. A closer examination of the spectrum of a "single-frequency" source as used in the FDTD method is in order to correctly interpret results in later chapters.

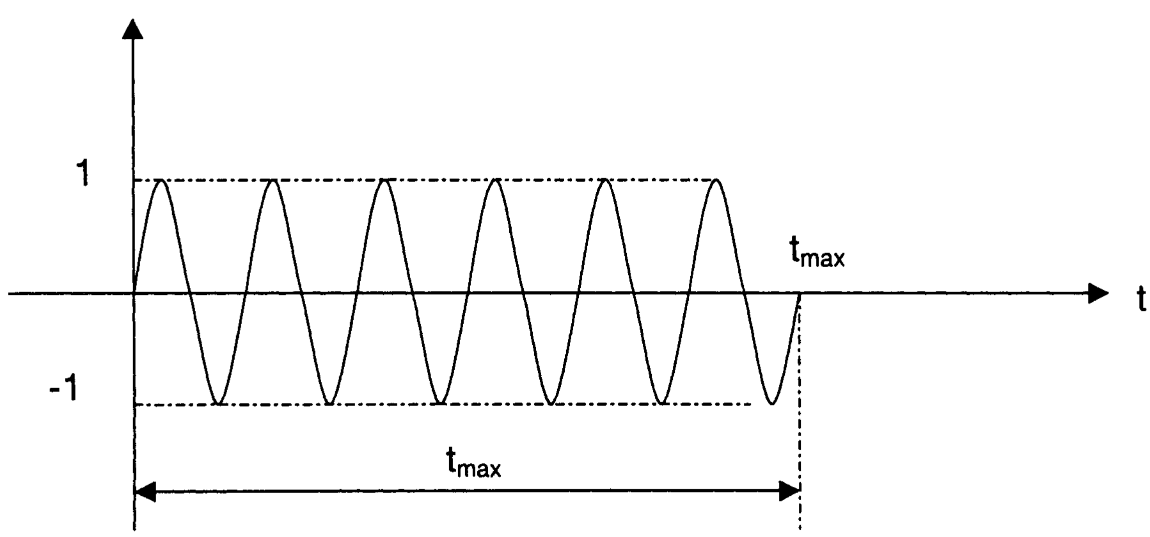

Figure 2.2 Causal "Single-Frequency" FDTD Source

In FDTD simulations only causal sources should be used. This means that the source signal, be it an electric current density acting as a source (and exciting a resultant incident field) or a directly specified field, the source will be zero for $t < 0$. Thus a "single-frequency" source (of frequency f_s, so that $\omega_s = 2\pi f_s$) will be as sketched in Figure 2.2. It turns on at $t = 0$ and lasts for a duration t_{max}, after which it is once more zero. If we represent this source signal by

$$f(t) = \begin{cases} \sin \omega_s t & 0 \le t \le t_{\max} \\ 0 & t < 0 \end{cases} \tag{2-15}$$

then we can view this as the multiplication of a rectangular pulse existing between $t = 0$ and $t = t_{max}$ with the sinusoid. In other words,

$$f(t) = f_1(t) \cdot f_2(t)$$

$$f_1(t) = \begin{cases} 1 & 0 \le t \le t_{\max} \\ 0 & t < 0 \end{cases} \tag{2-16}$$

$$f_2(t) = \sin \omega_s t \qquad -\infty < t < +\infty \tag{2-17}$$

The spectrum (i.e. Fourier transform) of the source signal is then the convolution of the transforms of the above shifted (to be causal) baseband pulse and the sinusoid. The individual Fourier transforms are found to be

$$F_1(\omega) = 2e^{-j\omega t_{\max}/2} \cdot \sin c(\frac{\omega t_{\max}}{2\pi}) \tag{2-18}$$

and

$$F_2(\omega) = (-j\omega) \cdot \left[\pi\delta(\omega - \omega_0) + \pi\delta(\omega + \omega_0)\right] \tag{2-19}$$

The convolution of the individual transforms leads to

$$F(\omega) = e^{-j(\omega-\omega_s)t_{max}/2} \cdot \{\sin c[\frac{(\omega-\omega_s)t_{max}}{2\pi}] + \sin c[\frac{(\omega+\omega_s)t_{max}}{2\pi}]\} \tag{2-20}$$

Its amplitude is

$$|F(\omega)| = \left| \sin c[\frac{(\omega-\omega_s)t_{max}}{2\pi}] + \sin c[\frac{(\omega+\omega_s)t_{max}}{2\pi}] \right| \tag{2-21}$$

and is plotted in Figure 2.3 for the case t_{max} = 3.856ns and f_s = 10 GHz. We observe that while a true (infinite duration) sinusoid of frequency f_s would have a spectrum consisting of a single spectral line at $f = f_s$, this is not the case for the finite duration signal. There is a maximum at $f = f_s$, but additional frequency components are present (some smaller amplitude spectral lines on either side of $f = f_s$ are just –13.2dB lower). If we increase the duration to t_{max} = 15.424ns, the signal spectrum is now that shown in Figure 2.4. A physical interpretation is easy. The longer the duration of the source signal the more it "looks" like a single-frequency sinusoid; the "spectral line" at $f = f_s$ is sharper. The smaller amplitude spectral components on wither side of $f = f_s$ are now closer to f_s but have the same amplitude before. This understanding will be important in the interpretation of results obtained using the FDTD in later chapters, and is the reason we have elaborated on the issue here. Notice that Figures 2.3(a) and 2.3(b) are the spectra for the same duration t_{max}; the only way they differ is in the plotting thereof we used more closely spaced points on the frequency axis in (b) then in (a). The spectra appear to differ in the vicinity of 8GHz, for example. It is important to realize that this is a "plotting phenomenon" only and must be kept in mind when drawing conclusions from such plots.

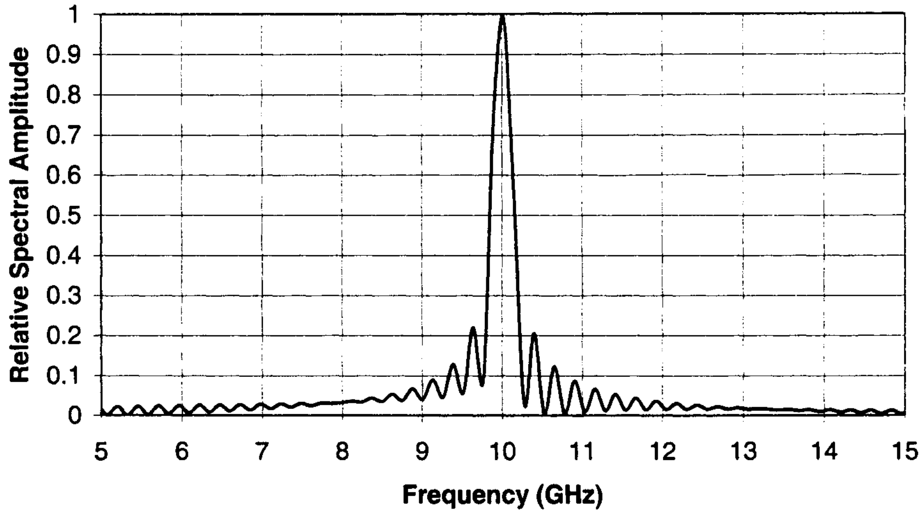

(a)

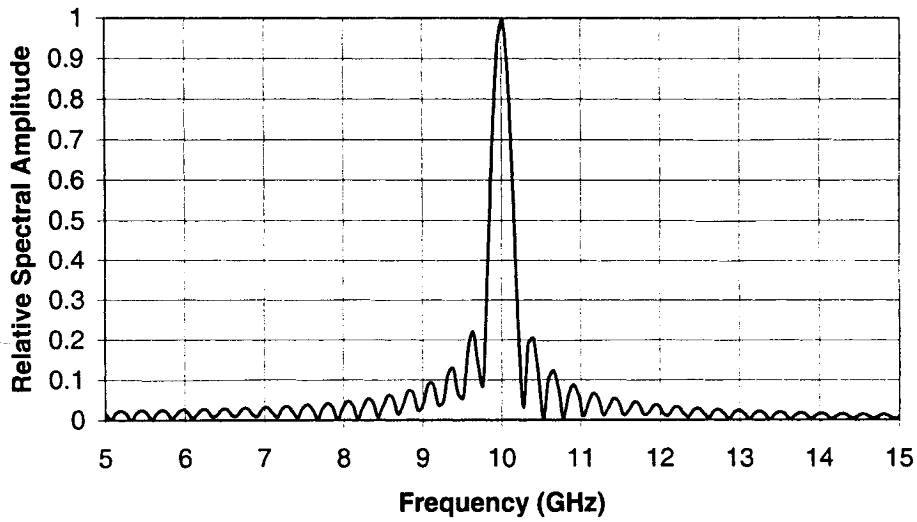

(b)

Figure 2.3 Fourier Transform of the Finite Duration "Single-Fequency" Source (f_s = 10 GHz & t_{max} = 3.856ns)
(a). Plot Obtained Using Points Spaced 0.12677 GHz Apart
(b). Plot Obtained Using Points Spaced 0.063385 GHz Apart

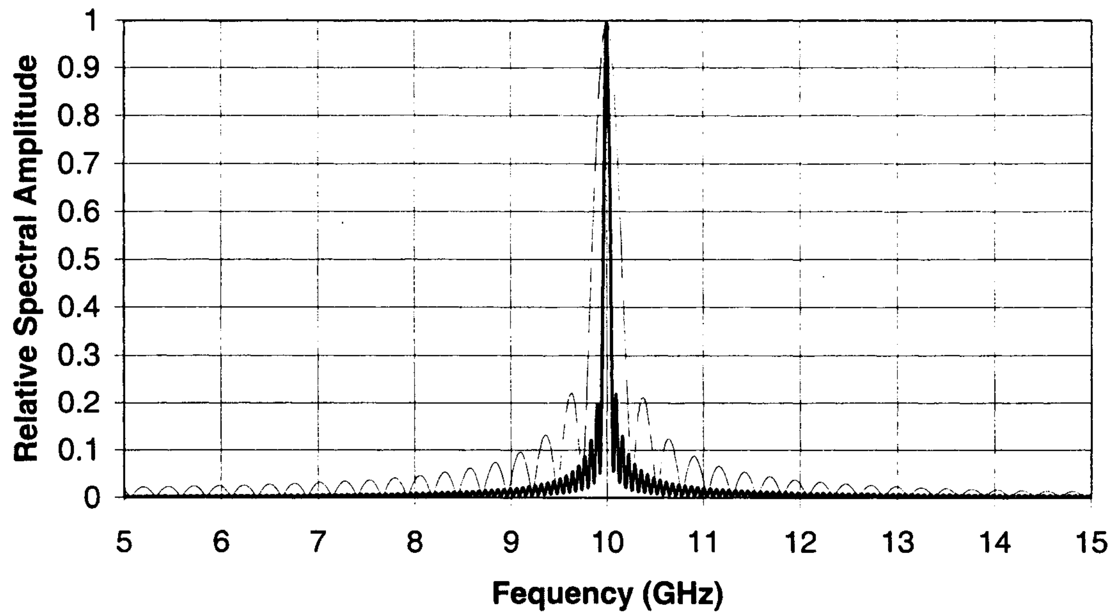

Figure 2.4 Fourier Transform (——) of the Finite Duration "Single-Fequency" Source (f_s = 10 GHz & t_{max} = 15.424 ns). The Dashed Line is the Spectrum Shown in Figure 2.3(b).

2.4.3 Restricting the Source and Material Property Time-variation

Since the FDTD method is a time-domain technique the outputs are electromagnetic field values at points in space as a function of time, such as $\overline{E}(x,y,z,t)$ and $\overline{H}(x,y,z,t)$. Any secondary parameters computed from these field values will thus also be time-domain quantities. All quantities of interest can be observed at each position in space as a function of time as the simulation progresses. Although the FDTD approach used in this thesis can be used for arbitrary time-variations of both the sources and the material properties, we will use the finite duration causal sinusoid discussed above. In addition, in order to be able to establish the correctness of the computed responses in the absence of related analytical or experimental results we will in this thesis restrict the material property selected to vary with time in a periodic fashion. Thus the systems under study will have a periodic (albeit not single-frequency) response, and it will make sense to talk about a steady state. We will always allow the source to be turned on for a sufficiently large duration t_{max} that the system under examination is able to reach this steady state. This steady-state will then be examined using either the instantaneous frequency concept or the signal spectrum, or both.

2.5 A REVIEW OF EXISTING ANALYSES OF THE ELECTROMAGNETIC BEHAVIOUR OF INDEPENDENTLY TIME-VARYING SYSTEMS

There is relatively little available in the literature on the subject of electromagnetic waves in independently time-varying media. The problem of electromagnetic wave propagation in a non-conducting medium whose permittivity and permeability vary with time was studied by Morgenthaler [6]. He considered plane wave incidence on an infinite slab of material of finite thickness. Approximate solutions to the associated electromagnetic model were obtained for permittivities with sinusoidal time-variation and constant permeability, with

$$\varepsilon\,(t) = \varepsilon_0 \varepsilon_{r0}(1 + b \sin \omega_m t) = \varepsilon_0\, \varepsilon_r(t) \qquad (2\text{-}22)$$

giving the permittivity at all points in the material as a function of time. In (2-22) quantity ω_m is the modulation frequency, b the modulation depth, and ε_{r0} the relative dielectric constant of the slab at the chosen operating point. We will use these results in Chapter 3 against which to compared FDTD solutions for the same problem.

Felsen and Whitman [7] considered the problem of pulsed plane wave propagation in infinite time-varying dispersive and non-dispersive media (that is, all of space filled with the same medium). While their asymptotic solutions provided insight into global behaviour of such systems these are mathematically complicated and not easily extended to the more complex geometries that might arise in future design environments.

Fante [8] derived complicated expressions for the electric fields of a plane wave incident on a material half-space with time-varying permittivity. The permittivity is allowed to have a single step change from one value to another. He then uses this solution to approximate a continuously varying permittivity; the assumption is that this latter variation is sufficiently slow (with respect to the frequency of the incoming wave) that such an approximation is valid. Although approximate mathematical expressions are provided as solutions there is no discussion of what they "are saying".

Jiang [9] considered the radiation and propagation of electromagnetic waves from a time-harmonic sources in a so-called "suddenly created plasma" (that is, in a medium that initially has zero conductivity but then changes abruptly to a medium with non-zero conductivity). The same medium is considered to occupy all of space.

Several papers have been published on plane wave propagation in infinite so-called space-time periodic medium. If it is the permittivity that is being varied it would, for such media (in the infinite medium case) be written in the form

$$\varepsilon\ (t,z) = \varepsilon_0 \varepsilon_{r0}[1 + b\sin(\omega_m - k_m t)] = \varepsilon_0\ \varepsilon_r(t,z) \qquad (2\text{-}23)$$

where k_m is referred to as the "pump" wavenumber. Observe that ω_m and k_m are unrelated to the frequency of the "signal" wave. Closed-form analytical solutions for permittivity variation of the form (2-23) have been studied by Simon [10], Cassedy and Oliner [11], Hessel and Oliner [12], and Holberg and Kunz [13]. In all cases the medium is infinite. In [14] electromagnetic wave propagation in an infinite medium with an abrupt change in permittivity is similarly studied analytically. Radiation by a dipole antenna in such an infinite space-time medium has been examined by Elachi [15].

The drawback that the above analytical solutions have in common are :

- They are all applicable to selected idealised geometries and could not be applied to the more complicated geometries one would expect to find in future of real-world devices.
- They represent attempts at approximate closed-form solutions to the particular problems (often in the form of specific secondary quantities rather than the fields themselves). It is difficult to extract performance indices that might be of interest in design work if solutions to the electromagnetic field themselves are not available.

More recent analytical work on the topic exhibits these same limitations [16,17,18]. Taylor, Lam and Shumpert [22] use the FDTD method in a somewhat idealised two-dimensional problem of electromagnetic pulse scattering from a cylindrical rod in an infinitely long cylindrical waveguide. The conductivity of the medium in the waveguide is assumed to be linearly time-varying (a "ramp") but the permittivity is kept constant. It is interesting to note that the authors of [14] observe that "one may become perplexed trying to" physically interpret the output. In this thesis we will show how the instantaneous frequency concept and spectra, for example, can be used to provide increased understanding of the data obtruded by the FDTD method when used with time-varying media.

Harfoush and Taflove [20] have applied the FDTD method to the solution of the problem of plane wave scattering from a material half-space whose conductivity is sinusoidally time-varying. Comparisons of the FDTD solutions to their own analytical results were excellent. The FDTD approach has also been applied in to the case of plane wave propagation through infinite [21] and finite thickness [22] switched plasma media. The FDTD has not yet been used for electromagnetic wave propagation problems involving material with periodically varying permittivity.

The success of the FDTD modelling in the latter three references begs the question of whether the FDTD method might be a useful general electromagnetic simulation tool for future finite-sized devices which utilise material with time-varying properties (specifically permittivities). We wish to demonstrate in this thesis that this is indeed so.

2.6 CONCLUSIONS

The essence of the finite-difference time-domain (FDTD) full wave electromagnetic analysis method was presented in this chapter. This thesis is concerned with examining and demonstrating the workability of this method for electromagnetic modeling in the presence of materials with independently time-varying properties. We indicated that by using a causal sinusoidal source of sufficiently long duration, and by restricting the time-variation of material properties to be periodic, the systems under study would possess a steady state. This will allow us to use the signal spectrum or the instantaneous frequency concept as a means of displaying, interpreting, and evaluating the correctness of the FDTD simulations that will be performed.

2.7 REFERENCES FOR CHAPTER 2

[1] J. van Bladel, "Electromagnetic Fields" (Hemisphere Publ. Co., 1985).

[2] C. A. Balanis, *Advance Engineering Electromagnetics*, New York, John Wiley & Son, 1989.

[3] E.J.Rothwell & M.J.Cloud, *Electromagnetics* (CRC Press, 2001).

[4] K.S.Yee, "Numercial solution of initial boundary value problems involving Maxwell's equations in isotropic media", IEEE Trans. Antennas Propagat., Vol.14, pp.302-307, Sept.1966.

[5] A.Taflove & S.C.Hagness, "Computational Electrodynamics : The Finite-Difference Time-Domain Method" (Artech House Inc., 2000) 2nd Edition.

[6] F. R. Morgenthaler,"Velocity Modulation of Electromagnetic Waves," *IRE Trans. Microwave Theory Tech.*, vol. 6, pp. 167-172, Apr. 1958.

[7] L.Felsen & G.M.Whitman, "Wave propagation in time-varying media," *IEEE Trans. Antennas Propagat.*, Vol. 18, pp.242-253, March 1970.

[8] R. L. Fante, "Transmission of Electromagnetic Waves into Time-Varying Media," *IEEE Trans. Antennas Propagat*, vol. 19, pp. 417-424, May 1971.

[9] C.Jiang, "Wave propagation and dipole radiation in a suddenly created plasma", *IEEE Trans. Antennas Propagat.*, Vol.23, No.1, pp.83-90, Jan.1975.

[10] J.C.Simon, "Action of a progressive disturbance on a guided electromagnetic wave", *IRE Trans. Microwave Theory Tech.*, Vol.8, pp.18-29, Jan.1960.

[11] E.S.Cassedy & A.A.Oliner, "Dispersion relations in time-space periodic media : Part I – Stable interactions", Proc.IEEE, Vol.51, pp.1342-1359, Oct.1963.

[12] A.Hessel & A.A.Oliner, "Wave propagation in a medium with a progessive sinusoidal disturbance", *IRE Trans. Microwave Theory Tech.*, Vol.6, pp.337-343, July 1961.

[13] D. E. Holberg and K. S. Kunz, "Parametric Properties of Fields in a Slab of Time-Varying Permittivity," *IEEE Trans. Antennas Propagat.*, vol. 14, pp. 183-194, March 1966.

[14] T. Ruiz, L. Wright, and J. Smith., "Characteristics of Electromagnetic Waves Propagating in Time Varying Media," *IEEE Trans. Antennas Propagat.*, vol. 26, pp. 358-361, Mar. 1978.

[15] C.Elachi, "Dipole antenna in space-time periodic media", *IEEE Trans. Antennas Propagat.*, Vol. 20, pp. 280-287, May 1972.

[16] A.G.Nerukh, I.V.Scherbatko & D.A.Nerukh, "Using evolutionary recursion to solve an electromagnetic problem with time-varying parameters", Microwave Opt. Tech. Letters, Vol.14, No.1, pp.3136, Jan.1997.

[17] A.G.Nerukh, I.V.Scherbatko & M.Marciniak, "The possible mechanism for a frequency shift by a time-varying of medium features", J. Telecommunications & Information Technology, Vol.1, pp.46-51, 2000.

[18] D.K.Kalluri, "Effect of switching a magnetoplasma medium on a travelling wave : Longitudinal propagation", *IEEE Trans. Antennas Propagat.*, Vol. 37, No.12, pp.1638-1642, Dec.1989.

[19] G. D. Taylor, D. H. Lam, Thomas and H. Shumpert, "Electromagnetic Pulse Scattering in Time-Varying Inhomogeneous Media," *IEEE Trans. Antennas Propagat.*, vol. 17, pp. 585-589, Sept. 1969.

[20] F.A.Harfoush & A.Taflove, "Scattering of electromagnetic waves by a material half-space with a time-varying conductivity", *IEEE Trans. Antennas Propagat.*, Vol. 39, No.7, pp.898-906, July 1991.

[21] J.H.Lee, D.K.Kalluri & G.C.Nigg, "FDTD simulation of electromagnetic transformation in a dynamic magnetised plasma", Int. J. Infrared & Millimeter Waves, Vol.21, pp.1223-1253, August 2000.

[22] D.K.Kalluri, J.H.Lee & M.M.Ehsan, "FDTD simulation of electromagnetic pulse interaction with a switched plasma slab", Int. J. Infrared & Millimeter Waves, Vol.24, pp.349-365, March 2003.

CHAPTER 3

FDTD Analysis of a Monochromatic Plane Wave Incident on a Dielectric Slab with Independently Time-Varying Permittivity

3.1 INTRODUCTION

The problem considered in this chapter is that of a monochromatic plane wave (of input "signal" frequency f_s) normally incident on a dielectric slab whose relative permittivity $\varepsilon_r(t)$ is considered to be independently time-varying. The geometry and several other features are shown in Figure 3.1. This is a one-dimensional problem for which at least some analytical solutions are available with which we can directly compare the FDTD predictions.

3.2 APPROXIMATE CLOSED-FORM ANALYSIS OF A PLANE WAVE INCIDENT ON A DIELECTRIC SLAB WITH SINUSOIDALLY TIME-VARYING PERMITTIVITY

We refer to the geometry shown in Figure 3.1. An incident plane electromagnetic wave traveling in the +x direction is represented as

$$E^{inc}(x,t) = E_o \sin\left\{\omega_s\left(t - \frac{x}{v}\right)\right\} \tag{3-1}$$

where ω_s is the frequency of the incident plane wave signal, E_0 is its amplitude, and v is the velocity of the plane wave. The quantities x and t are the spatial and temporal variables, respectively. The slab thickness is denoted as L. The permeability is the same as that of free space and the conductivity is zero. The slab permittivity has a sinusoidal variation with time of the form

$$\varepsilon\,(t) = \varepsilon_0 \varepsilon_{r0}(1 + b \sin \omega_m t) = \varepsilon_0\, \varepsilon_r(t) \qquad (3\text{-}2)$$

where ω_m is the modulation frequency, b the modulation depth, and ε_{r0} is the relative dielectric constant of the slab at the chosen operating point.

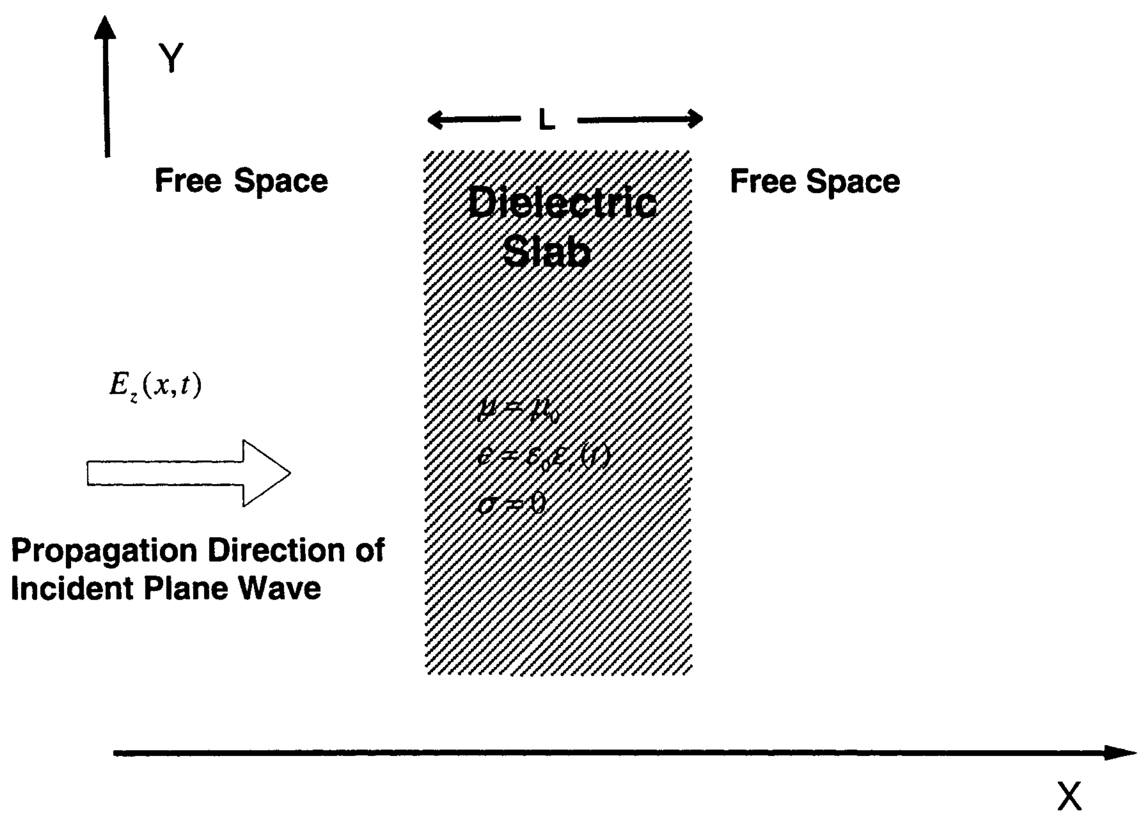

Figure 3.1 Plane Wave Incidents on a Dielectric Slab with Time-Varying Permittivity $\varepsilon\,(t)$. The Medium on Either Side of the Slab is Free Space.

Analytical work on this problem has been described by Morgenthaler [1], and will be used here against which to judge the success of the FDTD modeling of the same problem. In this section we will therefore summarise what has been said in [1].

The equation for a planar wavefront propagating with non-constant velocity can be written as

$$E\ (x,t) = E_o \sin\left\{\omega_s \left(t - \int \frac{dx}{v}\right)\right\} \tag{3-3}$$

We define the transit time as

$$T = \int \frac{dx}{v} \tag{3-4}$$

The total phase of the wave is defined as

$$\Phi = \omega_s \left(t - \int \frac{dx}{v}\right) \tag{3-5}$$

The instantaneous frequency is defined as

$$\omega(t) = \frac{d\Phi}{dt} = \omega_s \left(1 - \frac{dT}{dt}\right) \tag{3-6}$$

If the width of the dielectric slab is electrically thin, we can say [1] that the velocity can be approximated as constant for any given wavefront and dependent only upon the time t_o at which the wavefront first strikes the slab. Under this assumption the transit time becomes [1]

$$T = \int_0^L \frac{dx}{v(t)} \approx \frac{L}{v(t_o)} \tag{3-7}$$

and the instantaneous frequency can be approximated as [1]

$$\omega(t) \cong \omega_s \left(1 + \frac{L}{v(t)^2} \frac{dv(t)}{dt}\right) \tag{3-8}$$

In the case of the sinusoidal modulation of the permittivity as in (3-2), we can calculate the velocity to be

$$v(t) = \frac{1}{\sqrt{\varepsilon_{r0}\varepsilon_0\mu_0(1+b\sin\omega_m t)}} \tag{3-9}$$

Then the instantaneous frequency of the wavefront at the point where it emerges from the dielectric slab can be approximated as [1]

$$\begin{aligned} \omega(t) &\approx \omega_s\left[1-\frac{bL}{2v_0}\cdot\frac{\cos\omega_m t}{\sqrt{1+b\sin\omega_m t}}\right] \\ \Delta\omega &= -\frac{bL\omega_m\omega_s\cos\omega_m t}{2v_0\sqrt{1+b\sin\omega_m t}} \end{aligned} \tag{3-10}$$

where $v_0 = \dfrac{1}{\sqrt{\varepsilon_{r0}\mu_0\varepsilon_0}}$.

If the slab is electrically thick, so that the velocity cannot be assumed constant over the transit time interval, the transit time for the entire length L is given by [1]

$$T = \int_0^L \frac{dx}{v(t)} = t_1 - t_0 \tag{3- 11 }$$

In above equation, t_0 is the entrance time of a wavefront and t_1 the exit time of the same wavefront. In the case of sinusoidal permittivity modulation (3-2) the instantaneous frequency may then be approximated, for $b^2 << 2$, as [1]

$$\omega(t) \cong \frac{\sec^2(\frac{\omega_m t}{2})}{\left[1+\left\{\frac{2\tan(\frac{\omega_m t}{2})+b}{\sqrt{4-b^2}}\right\}^2\right]} \times \frac{\sec^2\left[\tan^{-1}\left\{\frac{2\tan(\frac{\omega_m t}{2})+b}{\sqrt{4-b^2}}\right\}-\frac{\omega_m L\sqrt{4-b^2}}{}\right]\omega_c}{\left[1+\left\{\frac{\sqrt{4-b^2}}{2}\tan\left[\tan^{-1}\left\{\frac{2\tan(\frac{\omega_m t}{2})+b}{\sqrt{4-b^2}}\right\}-\frac{\omega_m L\sqrt{4-b^2}}{}\right]-\frac{b}{2}\right\}^2\right]} \tag{3-12}$$

Values of L that are solutions of the equation

$$(\omega_m L\sqrt{4-b^2})/4v_0 = p\pi \qquad (\mathrm{p} = 0,1,2,3\ldots) \tag{3-13}$$

result in an instantaneous frequency that is constant and equal to ω_c. Such lengths are referred to as "null lengths" by Morgenthaler [1], and are given by

$$L = \frac{4p\pi v_0}{\omega_m\sqrt{4-b^2}} \qquad (\mathrm{p} = 0,1,2,3,\ldots) \tag{3-14}$$

The above analytical solutions will be used in Sections 3.5 and 3.6 to validate the FDTD analysis.

3.3 FDTD PROCEDURE FOR THE ANALYSIS OF A PLANE WAVE INCIDENT ON A DIELECTRIC SLAB OF ARBITRARILY TIME-VARYING PERMITTIVITY

In order to model above one-dimensional slab problem using the FDTD method [2], we may without loss of generality assumed a linearly-polarized electric field $E_z(x,t)$, with which will be associated a magnetic field $H_y(x,t)$. We will only vary the permittivity as a function of position or time. The conductivity of all materials is assumed to be zero, and the permeability to be that of free space. The Maxwell curl equations in the dielectric slab then reduce to

$$\begin{aligned} &\frac{\partial}{\partial t} H_y(x,t) = \frac{1}{\mu_0}\frac{\partial}{\partial x} E_z(x,t) \\ &\frac{\partial}{\partial t}\varepsilon(x,t) E_z(x,t) = \frac{\partial}{\partial x} H_y(x,t) \end{aligned} \qquad (3\text{-}15)$$

If we utilize the Yee cell idea in this one-dimensional context we obtain the leap-frog time-stepping (updating) expressions for the above E_z and H_y components as

$$E_z\Big|_i^{n+1/2} = \left[\frac{\varepsilon\big|_i^{n-1/2}}{\varepsilon\big|_i^{n+1/2}}\right] E_z\Big|_i^{n-1/2} + \left[\frac{\Delta t}{\varepsilon\big|_i^{n+1/2}}\right]\cdot\left[\frac{H_y\big|_{i+1/2}^{n} - H_y\big|_{i-1/2}^{n}}{\Delta x}\right]$$

$$H_y\Big|_{i+1/2}^{n+1} = H_y\Big|_{i-1/2}^{n} + \frac{\Delta t}{\mu_o}\cdot\left[\frac{E_z\big|_{i+1}^{n+1/2} - E_z\big|_i^{n-1/2}}{\Delta x}\right] \qquad (3\text{-}16)$$

The index n refers to the time variable and index i to the spatial variable. Thus the notation in the updating equations implies that $H_y\big|_i^n = H_y(x = i\Delta x, t = n\Delta t)$, for example.

Figure 3.2 shows how the fields E_z and H_y are interleaved in space and time. The updating equations are used to compute the field sequentially.

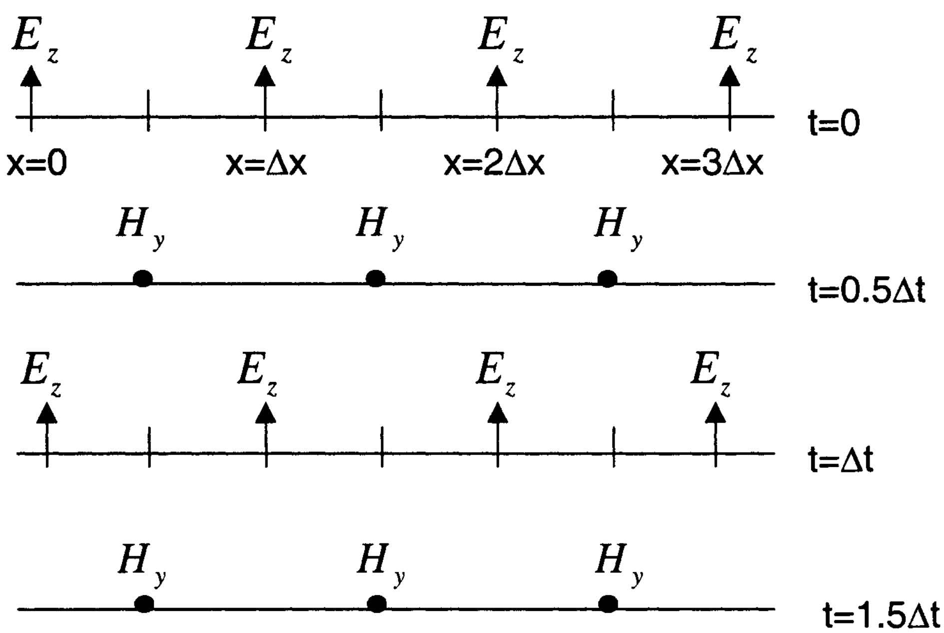

Figure 3.2 Leapfrog Method for One-Dimensional FDTD Simulation

The complete FDTD set-up for the problem at hand is illustrated in Figure 3.3. The impressed soft source is located at $x = x_s$ (index $k = k_s$ on the FDTD grid) and is implemented as in [8] through use of the following updating equation for the electric field at location $k = k_s$ and magnetic field at $k = k_s - ½$

$$E_z\Big|_{k_s}^{n+1/2} = \left[\frac{\varepsilon\big|_{k_s}^{n-1/2}}{\varepsilon\big|_{k_s}^{n+1/2}}\right] E_z\Big|_{k_s}^{n-1/2} + \left[\frac{\Delta t}{\varepsilon\big|_{k_s}^{n+1/2}}\right]\cdot\left[\frac{H_y\big|_{k_s+1/2}^{n} - H_y\big|_{k_s-1/2}^{n}}{\Delta x}\right] + E_{source_z}\Big|_{k_s}^{n+1/2}$$

$$H_y\Big|_{k_s-1/2}^{n+1} = H_y\Big|_{k_s-1/2}^{n} + \left[\frac{\Delta t}{\mu\big|_{k_s-1/2}^{n+1}}\right]\cdot\left[\frac{E_z\big|_{k_s}^{n+1/2} - E_z\big|_{k_s-1}^{n-1/2}}{\Delta x} - E_{source_y}\Big|_{k_s}^{n+1/2}\right] \tag{3-17}$$

A word of explanation is in order. In this 1D formulation, when we have an incident incident electric field E_{source_z} at the specific point k_s, the adjacent two H fields at $k_s - 1/2$ and $k_s + 1/2$ will be affected first, and two incident wave will be generated [3], propagating in the +x and –x directions. If we want only one incident wave propagating in the +x direction we can subtracted the incident electric field from the updating equation for the magnetic field at position $k_s - 1/2$. Hence the form of the updating equation for the magnetic field in (3-17).

Absorbing boundary conditions (ABCs) are used to truncate the solution region at x = 0 and x = x_{max}. The one-dimensional FDTD implentation of the ABC at x = 0 is

$$E_z^{n+1}(0) = E_z^n(1) + \frac{v_{fs}\Delta t - \Delta x}{v_{fs}\Delta t + \Delta x}\cdot[E_z^{n+1}(1) - E_z^n(0)] \tag{3-18}$$

while that at x = x_{max} is

$$E_z^{n+1}(\max x) = E_z^n(\max x - 1) + \frac{v_{fs}\Delta t - \Delta x}{v_{fs}\Delta t + \Delta x}\cdot[E_z^{n+1}(\max x - 1) - E_z^n(\max x)] \tag{3-19}$$

where $v_{fs} = \dfrac{1}{\sqrt{\mu_0\varepsilon_0}}$ since the ABCs are located in free space.

At points on the interface between free space and the dielectric slab the question that always arises when using the FDTD method is what value of permittivity must be used in the updating equations (3-16). Numerical experiments have shown [2] that while, for the small values of Δx that have to be used with the FDTD anyway, it in many cases does not matter whether the free space or dielectric slab permittivity is used, the consensus is that so-called "media-averaging" should be applied for best results. This means that at points lying on the interface, the value of permittivity used in the updating equations should be the average value of the free space and dielectric slab permittivities, namely $\varepsilon_o(1+\varepsilon_r)/2$.

In almost all FDTD work described in the literature the material properties have not been independently time-varying. We have devised a versatile way of incorporating such time-varying properties that does not require changes to the FDTD updating equations if the material property's time dependence is altered. Once the function $\varepsilon_r(t)$ is known for a specific application, and the Δt of the FDTD algorithm has been selected, we draw up a table (in practice an array of numbers in the computer code) of relative permittivity values $\varepsilon_r(n) = \varepsilon_r(n\Delta t)$ which can be used in the update equations at the appropriate points in time $t = n\Delta t$. A similar thing can be done for the conductivity if it varies with time, and so on. Thus, with this approach, the FDTD can be seen to be a "natural" method to use when time-varying materials are involved. The properties could even vary differently at different locations in the solution region, and the look-up table approach would still apply.

Using the parameters specified in Table 3.1, we obtain the computed responses $E_z(x_o,t)$ as shown in Figures 3.4 and 3.5 for the electrically thin and electrically thick slabs, respectively. It is interesting to observe that, for the parameters selected, the thick slab acts principally as a phase modulator while the thin slab provides some amplitude modulation too. These results are indicative of the usefulness of being able to perform electromagnetic analysis in the time-domain using the FDTD method when time-varying materials are present. We will further demonstrate this in the remainder of this chapter. For these and later results it is noted that we always ensure that the spatial length of the cell (Δx) is such that the FDTD results have converged.

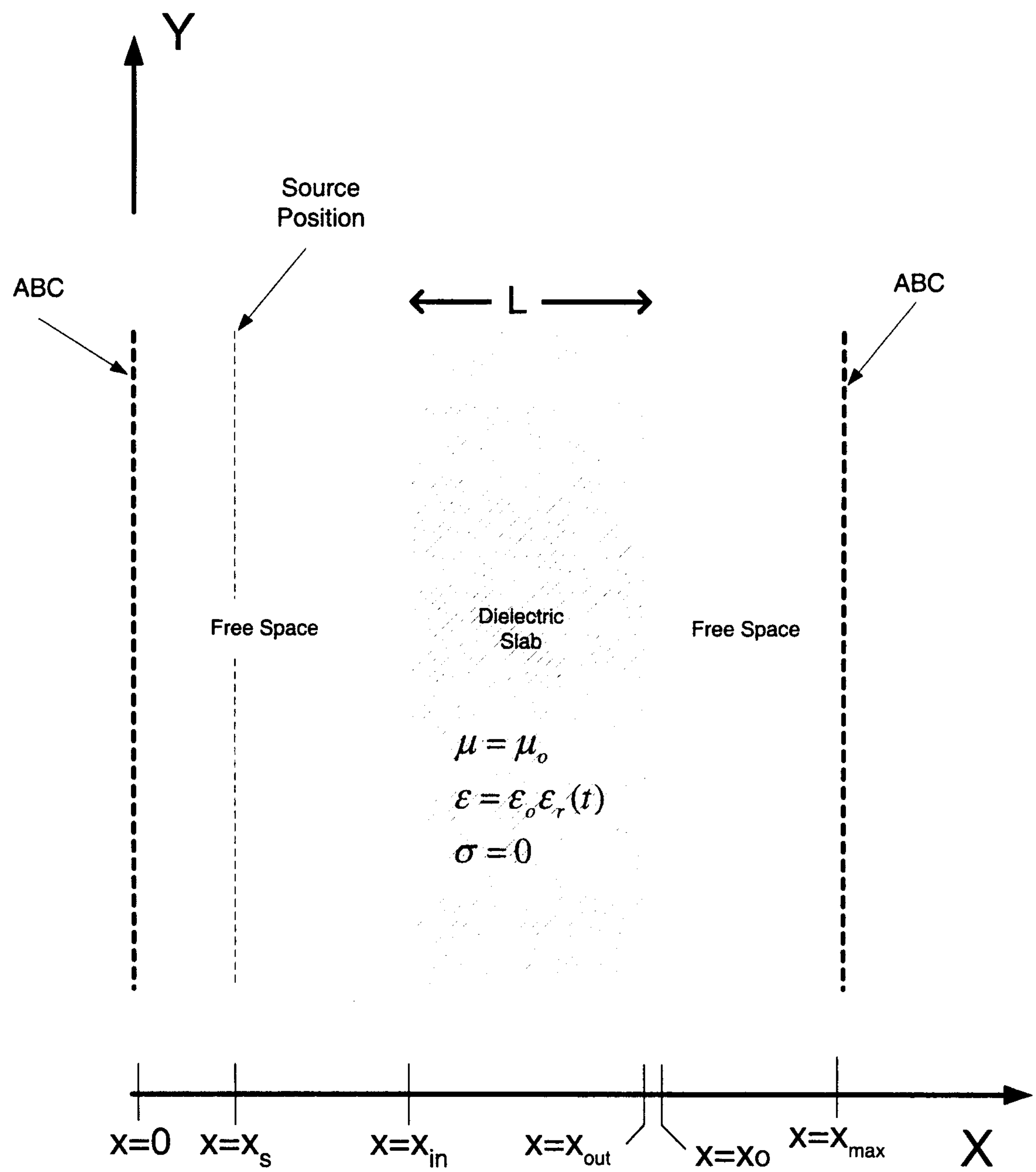

Figure 3.3 FDTD Model of the Time-Varying Dielectric Slab Problem

Table 3.1 Parameters Used for the Problem of Plane Wave Propagation Through a Dielectric Slab of Sinusoidally Time-Varying Permittivity

Quantity	*Description*	*Value*
Δx	Length of Cell	1.5 mm
Δt	Time Step	50 ps
ε_{ro}	Quiescent Relative Permittivity of the Dielectric Slab	3.0
$\varepsilon\ (t)$	Sinusoidally Time-Varying Permittivity	$\varepsilon\ (t) = \varepsilon_0 \varepsilon_{r0}(1 + b \sin \omega_m t)$
x_o	Location of Output Observation Point	$L + 2\Delta x$
L	Thickness of Dielectric Slab	93mm (Electrically Thin Slab) 3mm (Electrically Thick Slab)
ω_s	Frequency of Impressed Source	10 GHz $\times$ 2π
ω_m	Modulation Frequency	1 GHz $\times$ 2π

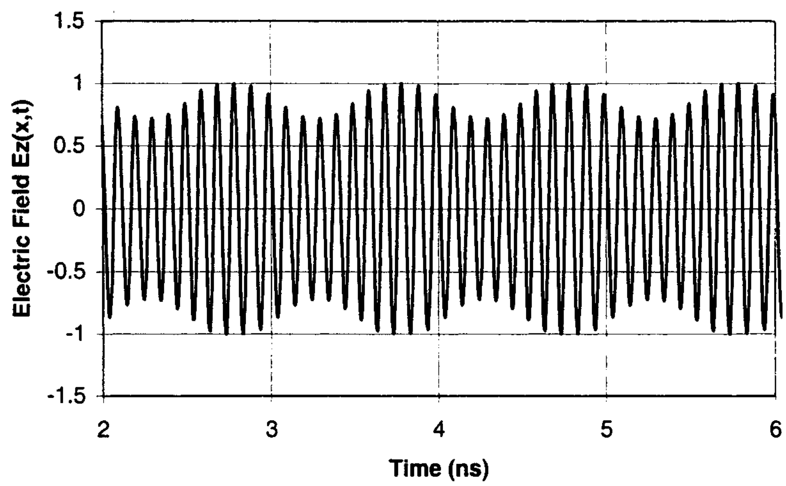

Figure 3.4 Electric Field $E_z(x_o, t)$ at $x_o = x_{out} + 2\Delta x$ as a Function of t for the Electrically Thin Slab. The Modulation Depth was b = 0.67.

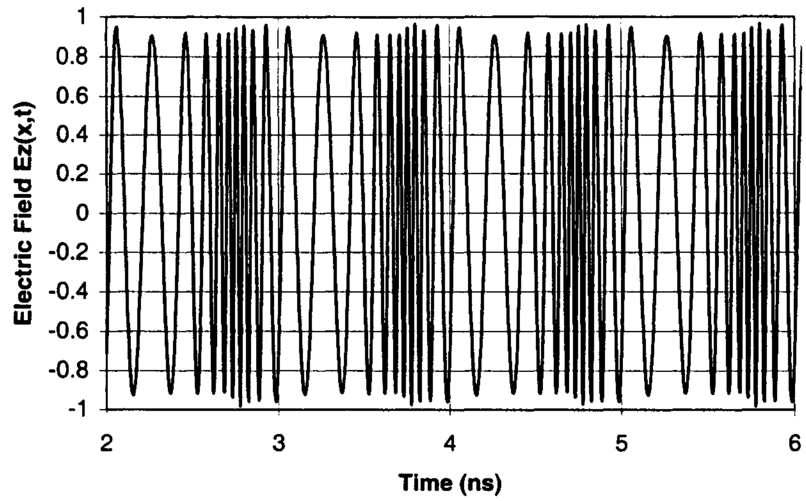

Figure 3.5 Electric Field $E_z(x_o,t)$ at $x_o = x_{out} + 2\Delta x$ as a Function of t for the Electrically Thick Slab. The Modulation Depth was b = 0.67.

3.4 A TECHNIQUE TO COMPUTE INSTANTANEOUS FREQUENCY USING THE FDTD OUTPUT

In order to make a direct comparison with the approximate analytical results of [1], which does not present solutions for electromagnetic field values but only the instantaneous frequency, it is necessary to determine the instantaneous frequency $\omega(t)$ from the FDTD output $g(t) = E_z(x_o,t)$ at some observation point $x = x_o$. Recall that the instantaneous frequency of a signal $g(t)$ is defined [4] as $\omega(t) = d\phi(t)/dt$, where $\phi(t)$ is the phase of $g(t)$. In the FDTD simulations $g(t)$ would be available in sampled form $g(n) = g(n\Delta t)$ where Δt is the FDTD time step. The question arises as to how the phase can be extracted from a time-domain method such as the FDTD simulations. We have devised a method that (with hindsight) is relatively straightforward, but which has not been described elsewhere.

The FDTD simulation is first executed using a source whose time-dependence is sinusoidal, of the form

$$f_{source}^{(1)}(t) = \begin{cases} \sin \omega_0 t & 0 \le t \le t_{\max} \\ 0 & t < 0 \end{cases} \tag{3-20}$$

with the FDTD output denoted $g^{(1)}(n) = g^{(1)}(n\Delta t)$. The simulation is then repeated, with all parameters identical except that the time-dependence of the source is now cosinusoidal, namely

$$f_{source}^{(2)}(t) = \begin{cases} \cos \omega_0 t & 0 \le t \le t_{\max} \\ 0 & t < 0 \end{cases} \tag{3-21}$$

and the output denoted $g^{(2)}(n) = g^{(2)}(n\Delta t)$. The sequence of phase values of the output signals is then given by

$$\phi\,(n) = \tan^{-1}\left[\frac{g^{(1)}(n)}{g^{(2)}(n)}\right] \tag{3-22}$$

where $\phi\,(n) = \phi\,(n\Delta t)$. The four-quadrant inverse tangent function (defined over angular range [-π,π], as for routine *atan2* [5]) should be used. The sequence of instantaneous frequency values can then be found using a variety of methods of estimating the numerical derivative of $\phi\,(n)$. An M-th order generalised phase difference estimator (that is, instantaneous frequency estimator) has been given by Boashash [4] as

$$\omega(n) = \sum_{m=-M/2}^{m=M/2} b_m \phi\,(n+m) \tag{3-23}$$

where $\omega\,(n) = \omega\,(n\Delta t)$, and the coefficients b_m are given in [4]. We have used a fourth-order estimator

$$\omega(n) \cong \frac{\phi\,(n-2) - 8\phi\,(n-1) + 8\phi\,(n+1) - \phi\,(n+2)}{12\Delta t} \qquad (3\text{-}24)$$

In essence, this "estimator" uses a five-point numerical derivative. The order of magnitude of the error is $O\{(\Delta t)^4\}$, and since the FDTD time step Δt is small this error will be very small.

3.5 EXAMINATION OF THE COMPUTED RESPONSE FOR A PLANE WAVE INCIDENT ON A DIELECTRIC SLAB OF SINUSOIDALLY TIME-VARYING PERMITTIVITY

A. *The Case of an Electrically Thick Slab*

In Figure 3.6 is shown a comparison of the FDTD-computed instantaneous frequency, and that determined using the approximate analytical expression (3-12) for a modulation depth b = 0.17. Figures 3.7 and 3.8 show similar results but for modulation depths b = 0.5 and b = 0.67, respectively.

Firstly, we observe that the modulation depth affects the maximum and minimum values assumed by the instantaneous frequency. We will henceforth refer to the difference between these maximum and minimum instantaneous frequency values as the "instantaneous frequency swing". In other words, the modulation depth is one of the factors that control the instantaneous frequency swing. Secondly, we note in Figure 3.6 that the agreement between the FDTD results and those using expression (3-12) is excellent. Note that for the case reported in this figure b^2 = 0.03 which satisfies the condition $b^2 << 2$ required for (3-12) to be accurate. In Figures 3.7 and 3.8 the agreement is not as good, no doubt because the latter condition is less closely satisfied.

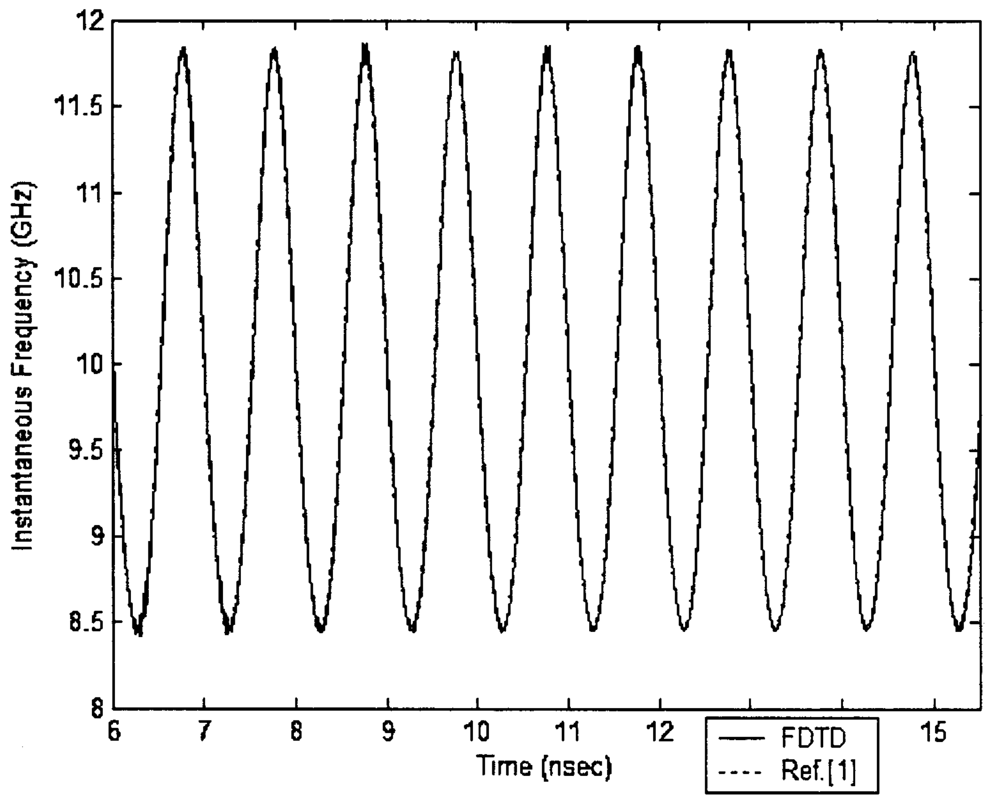

Figure 3.6 Instantaneous Frequency of the Electric Field $E_z(x_o, t)$ at $x_o = x_{out} + 2\Delta x$ as a Function of t for the Electrically Thick Slab. The Modulation Depth was b = 0.17. The FDTD Prediction (——) is Compared to the Analytical Prediction [1] (- - - -) Using Expression (3-12)

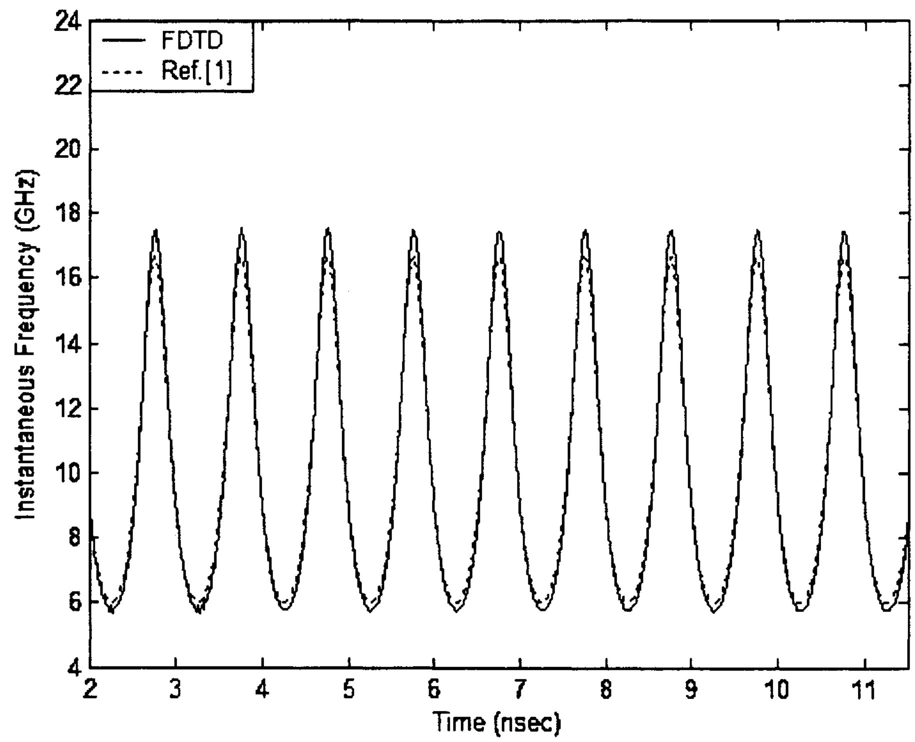

Figure 3.7 Instantaneous Frequency of the Electric Field $E_z(x_o,t)$ at $x_o = x_{out} + 2\Delta x$ as a Function of t for the Electrically Thick Slab. The Modulation Depth was b = 0.5. The FDTD Prediction (——) is Compared to the Analytical Prediction [1] (- - - -) Using Expression (3-12)

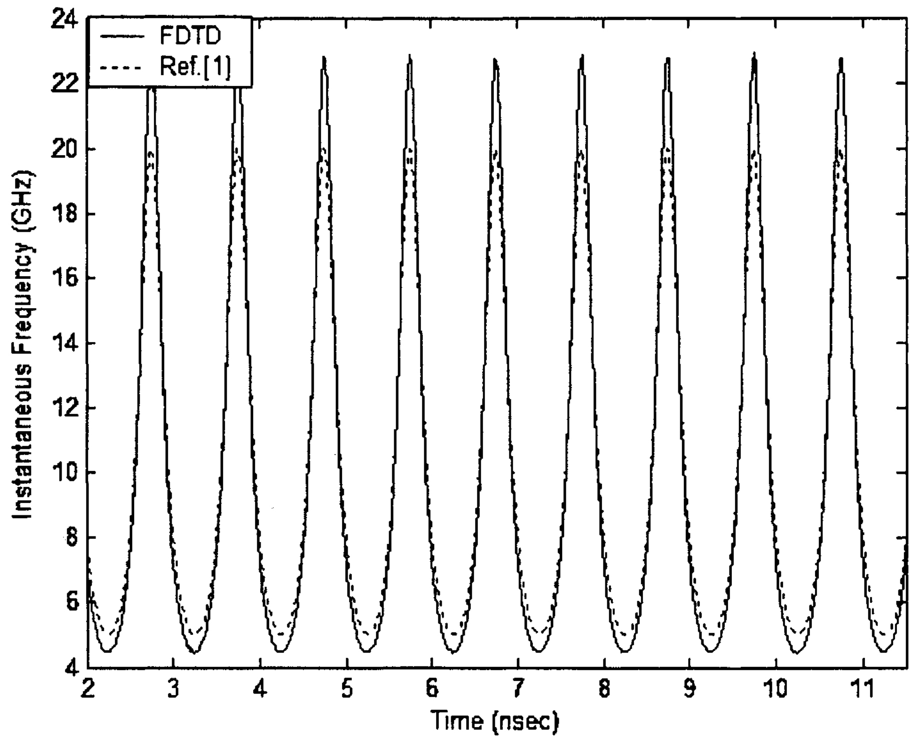

Figure 3.8 Instantaneous Frequency of the Electric Field $E_z(x_o,t)$ at $x_o = x_{out} + 2\Delta x$ as a Function of t for the Electrically Thick Slab. The Modulation Depth was b = 0.67. The FDTD Prediction (——) is Compared to the Analytical Prediction [1] (- - - -) Using Expression (3-12)

B. The Case of an Electrically Thin Slab

The instantaneous frequency swing for the electrically thin slab, with all conditions other than the slab thickness L kept the same as in Table 3.1 was computed using the FDTD model. The observations are much the same as for the electrically thick slab. Agreement between the FDTD results is closer for smaller values of the modulation depth b, which is observed to exercise control over the instantaneous frequency swing. However, as Figure 3.9 will bear witness, for the same value of b the amount of instantaneous frequency swing is less for the thin slab than the thicker one. Thus slab depth is clearly also a controlling factor. We will investigate this next.

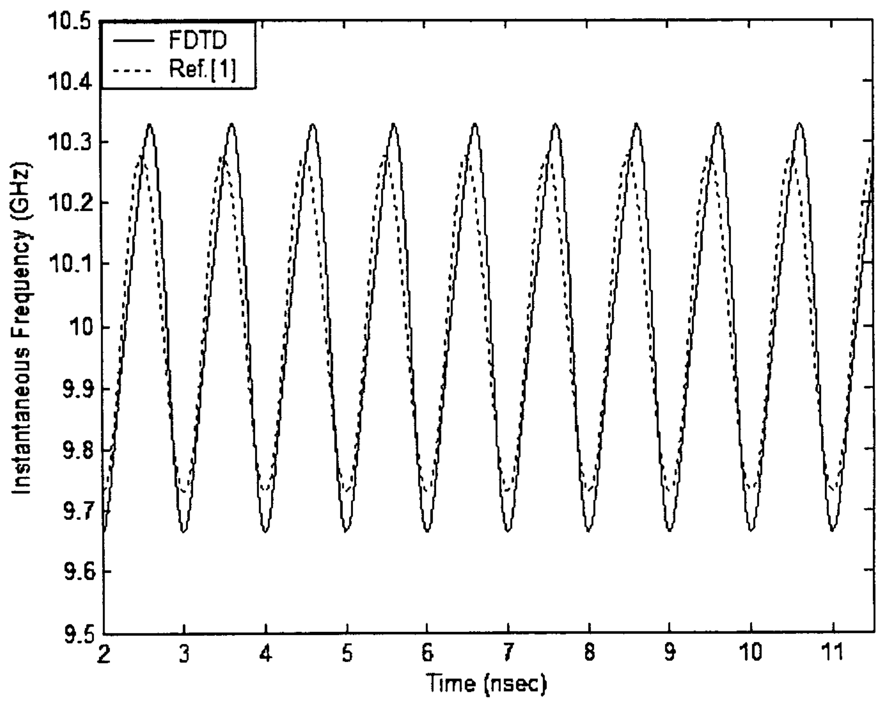

Figure 3.9 Instantaneous Frequency of the Electric Field $E_z(x_o,t)$ at $x_o = x_{out} + 2\Delta x$ as a Function of t for the Electrically Thin Slab. The Modulation Depth was b = 0.5. The FDTD Prediction (——) is Compared to the Analytical Prediction [1] (- - - -) Using Expression (3-10)

C. *The Influence of Slab Thickness on the Instantaneous Frequency Swing*

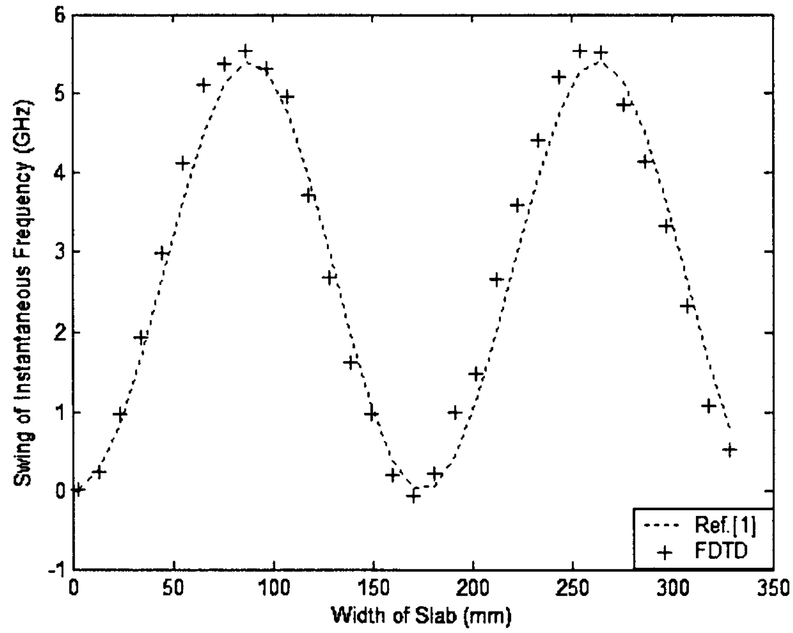

Figure 3.10 Predicted Instantaneous Frequency Swing Using the Electric Field $E_z(x_o,t)$ Observed at at $x_0 = L + 2\Delta x$ for Various Slab Widths. The Modulation Depth was b = 0.67. The FDTD Predictions (+) are Compared to the Analytical Prediction (——) .

The FDTD simulations were done for slabs of increasing thickness and the frequency swing extracted for each slab. The approximate analytical value for this swing was also calculated for each slab thickness. These predictions are compared in Figure 3.10. Except for a slight shift between the two graphs the agreement is excellent, with the FDTD computations possibly the more accurate of the two.

We can use expression (3-14) to predict the thickness of a "null length slab". With the order p = 1, f_m = 1GHz, ε_{r0} = 9.0, and b = 0.1111, expression (3-14) yields L_{null1} =0.1001m. Figure 3.11 shows the instantaneous frequency as a function of time for the above slab obtained using the FDTD method and the approximate analytical solution. As expected, the frequency swing is small. We observe that the FDTD result appears "noisy". We will examine this issue in Section 3.6. Before that we will draw some preliminary conclusions.

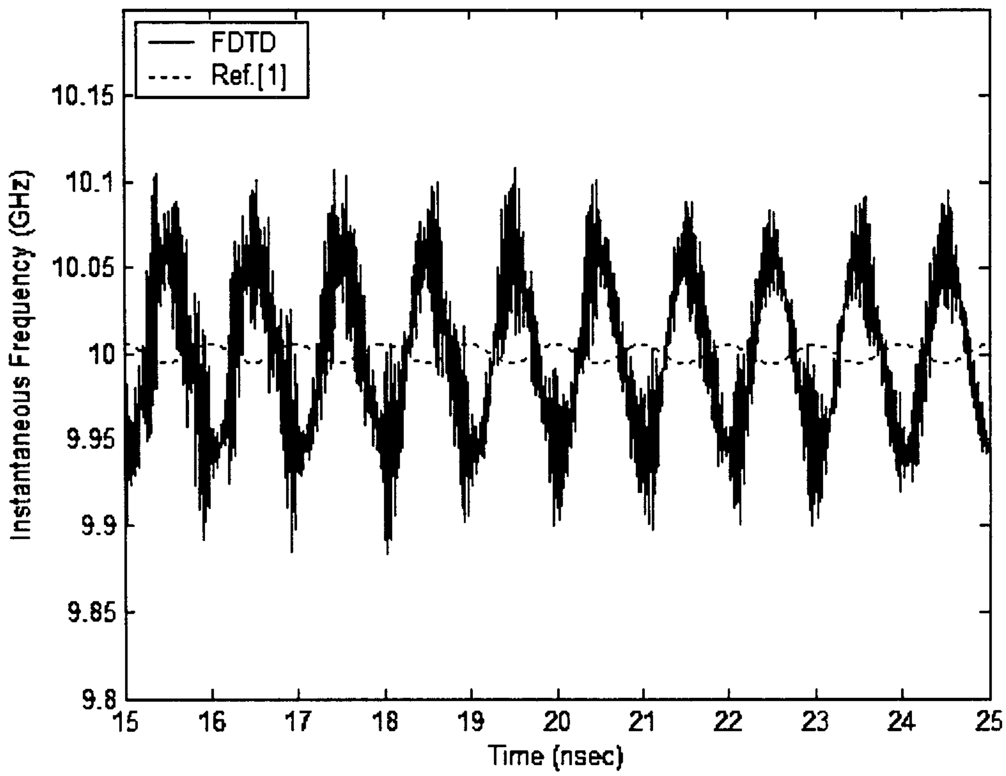

Figure 3.11 Comparison of the Calculated Instantaneous Frequency Using The FDTD Method and the Approximate Solution (Ref.[1]) for the Null Length Slab with Time- Varying Permittivity

D. A Preliminary Verdict on the Suitability of the FDTD Method for Electromagnetic Waves in Time-Varying Materials

The comparisons between the FDTD and approximate analytical results in Figures 3.6 through 3.8 showed that the FDTD results are identical to the analytical ones over the range of b values for which the analytical expressions are valid. As the vaues of b depart from the condition required by the analytical approximation the difference between the FDTD results and the analytical ones becomes larger. Furthermore, we saw in Figure 3.10, which revealingly showed the effect of the slab thickness, that the FDTD method predicts "null lengths" in agreement with the analytical solutions. We can conclude that the FDTD modelling provides correct results for the time-varying material problem considered, and that it is able to do so beyond the range over which the analytical solutions are able to do so.

When examining "unconventional" problems in electromagnetics, a class of problem into which the present one certainly falls, it is best to check as many aspects as possible. We therefore computed the instantaneous frequency for the case of thick slab using the FDTD values of the $E_z(x_o,t)$ at observation points x_o at increasing distances from the slab. Figures 3.12 and 3.13 show these results, and should be viewed in conjunction with Figure 3.8. Since all observation points are outside of the slab (at the "output" side) we should not see any change in the instantaneous frequency plots. A given instantaneous frequency should simply "occur at a later time" (the time taken for the frequency shifted wave to reach the further observation point). Thus as we proceed from Figure 3.8 to 3.12 to 3.13 we see the instantaneous frequency plots shift to the right (i.e. to later times).

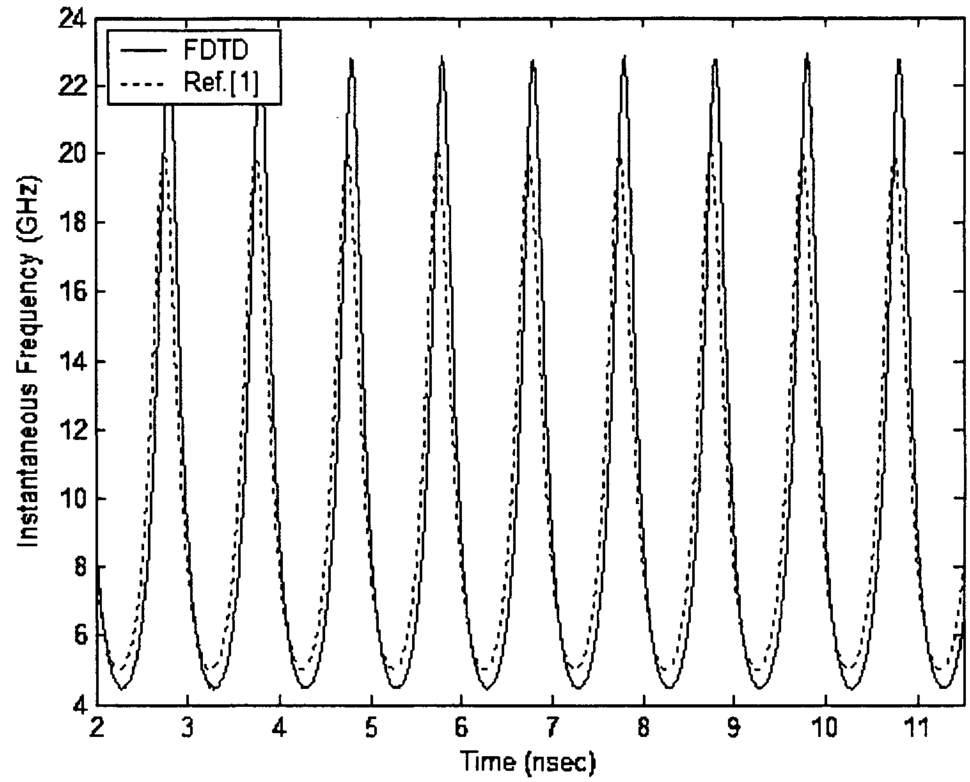

Figure 3.12 FDTD-Predicted Instantaneous Frequency (——) Obtained Using the Electric Field $E_z(x_o,t)$ Observed at $x_o = x_{out} + 10\Delta x$. The Modulation Depth was $b = 0.67$. The Analytical Prediction (- - - -) is Only Possible at $x_o = L + 2\Delta x$.

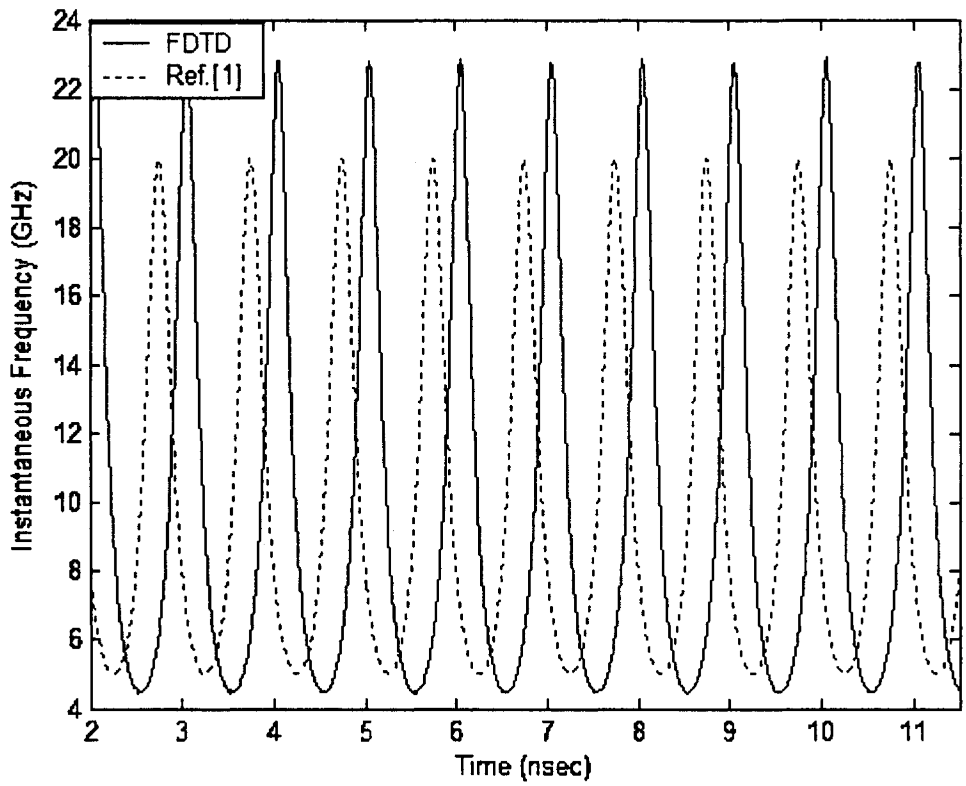

Figure 3.13 FDTD-Predicted Instantaneous Frequency (——) Obtained Using the Electric Field $E_z(x_o,t)$ Observed at $x_o = x_{out} + 60\Delta x$. The Modulation Depth was b = 0.67. The Analytical Prediction (- - - -) is Only Possible at $x_o = L + 2\Delta x$.

3.6 IMPROVED FDTD RESULTS USING POST-COMPUTATION FILTERING

The FDTD system is actually a sampling system, governed by the Nyquist-Shannon sampling theorem. This theorem states that, when sampling a signal at discrete intervals (Δt in this case), the sampling frequency must be greater than twice the highest frequency of the input signal in order to be able to reconstruct the original signal perfectly from the sampled data senquency. In the FDTD computations under discussion Δt = 50ns, and so the sampling freqeuncy is effectively $1/\Delta t$ = 200GHz. This means the highest frequency signal that can be faithfully accounted for on the FDTD lattice is $f_{max} = ½(1/\Delta t) =$ 100GHz. If we determine the spectrum of the signal at an observation point just outside the slab, and plot that portion of it which lies above 100 GHz, we obtain the result shown in Figure 3.14. There are clearly frequency components higher than 100GHz. We can remove these higher frequency components in the FDTD output passing it through a low pass filter. This is suggested in [6], although details are not provided there.

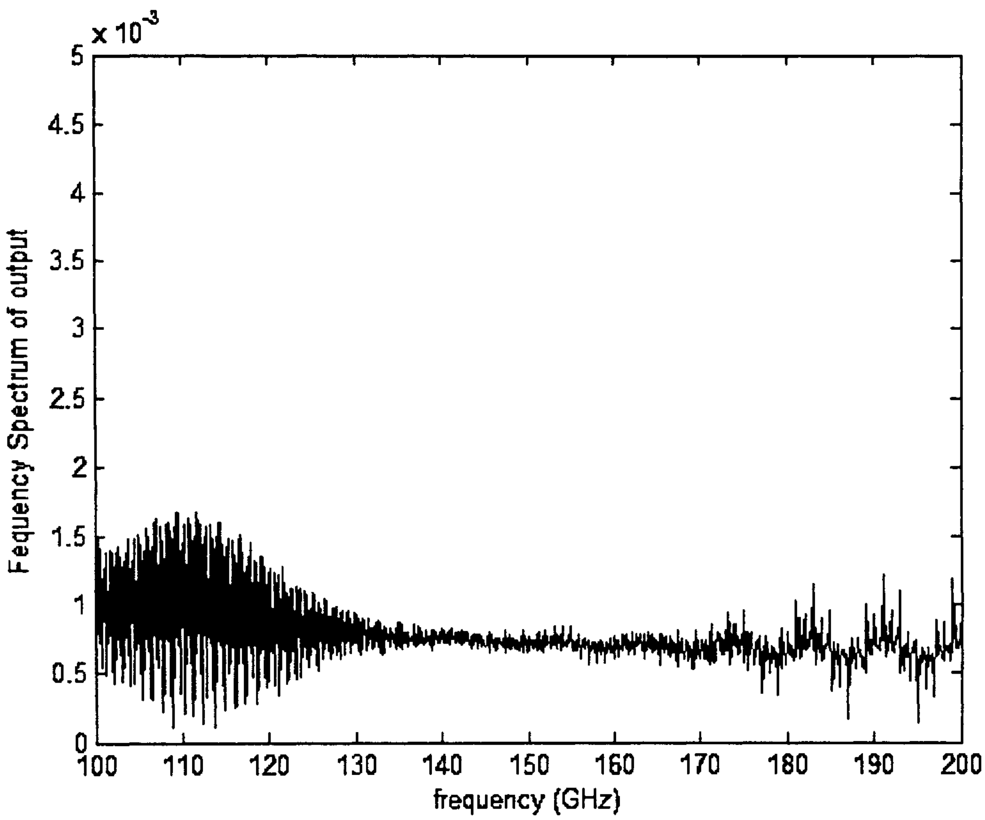

Figures 3.14 Spectrum at an Observation Point Just Outside the Slab

A digital filter low pass filter (to be specific, a Butterworth infinite impulse response realization due to their maximally flat property) was designed to exclude frequencies higher than the upper limit 100 GHz. We have used a filter operating at a sampling rate three times $1/\Delta t$ Hz with specifications shown in Table 3.2.

Table 3.2 Butterworth Low-Pass Filter Parameters

Parameter	Value
Passband Edge	$\frac{1}{2\Delta t}$ Hz
Sampling Frequency	$3\left(\frac{1}{\Delta t}\right)$ Hz
Stopband Edges	$0.9\left(\frac{1}{2\Delta t}\right)$ Hz
Passband Ripple	1dB
Minimum Stopband Attenuation	40 dB

The difference equation for the above filter, which is the form actually used on the sequence of FDTD field values, is

$$y(n) = \sum_{k=0}^{N} b_k x(n-k) + \sum_{k=1}^{N} a_k y(n-k) \tag{3-25}$$

where the coefficients b_m and a_m determine the response of the filter. We have used the commercially available routines for the filter design [7]. The coefficients of the filter are for reference listed in Table 3.3.

Table 3.3 Coefficients of the Butterworth Digital Low Pass Filter

b1	0.0000	**a1**	1.0000
b2	0.0000	**a2**	-5.4143
b3	0.0001	**a3**	15.2019
b4	0.0003	**a4**	-28.3370
b5	0.0010	**a5**	38.6495
b6	0.0023	**a6**	-40.4578
b7	0.0038	**a7**	33.3551
b8	0.0048	**a8**	-21.9438
b9	0.0048	**a9**	11.5699
b10	0.0038	**a10**	-4.8738
b11	0.0023	**a11**	1.6227
b12	0.0010	**a12**	-0.4185
b13	0.0003	**a13**	0.0808
b14	0.0001	**a14**	-0.0110
b15	0.0000	**a15**	0.0009
b16	0.0000	**a16**	-0.0000

When the previously discussed simulations (in Figure 3.8, for instance) are repeated with the filtering included the results do not look very different. However, if we magnify the upper portion of the graph in Figure 3.8 (in the vicinity of t = 9.75ns), as shown in Figure 3.15, we see that the filtering operation does indeed remove the erratic high-frequency components' behaviour which the FDTD is not able to reliably handle anyway.

If we add this filter to the null length slab computation shown in Figure 3.11 the result is as shown in Figure 3.16. The "noisyness" has been removed. However, we observe that there is a shift, along the time axis (towards later times), between the filtered and unfiltered instantaneous frequency versus time plot. This is likely due to the delay caused by the filter itself.

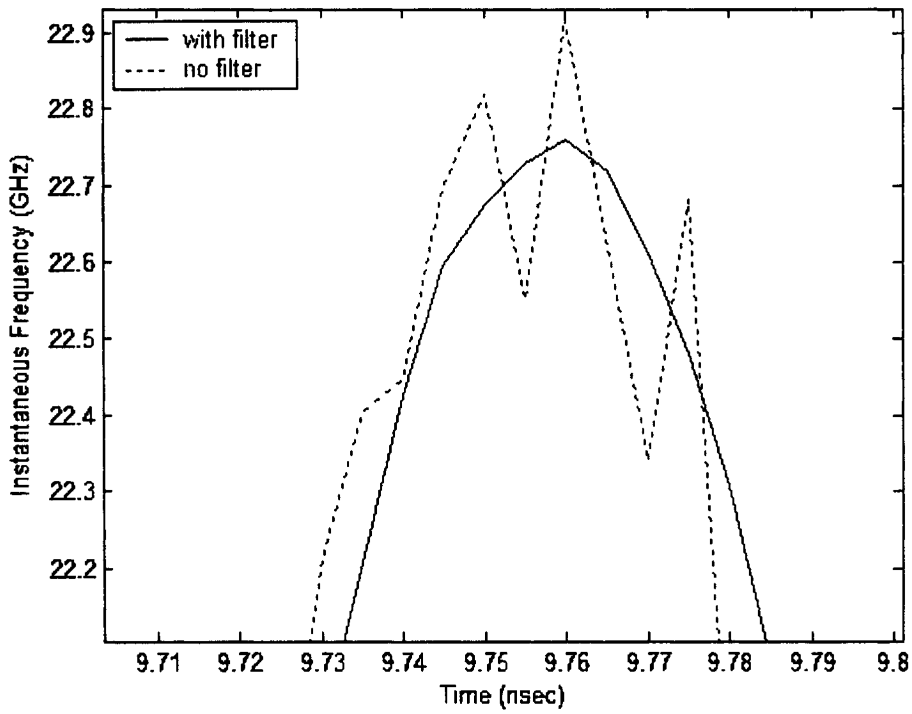

Figure 3.15 Magnified View of a Portion of the Graph in Figure 3.8. Both Results Shown were Obtained Using FDTD Modelling. The Unfiltered FDTD Result is Shown as the Dashed Line and the Filtered Result as the Solid Line

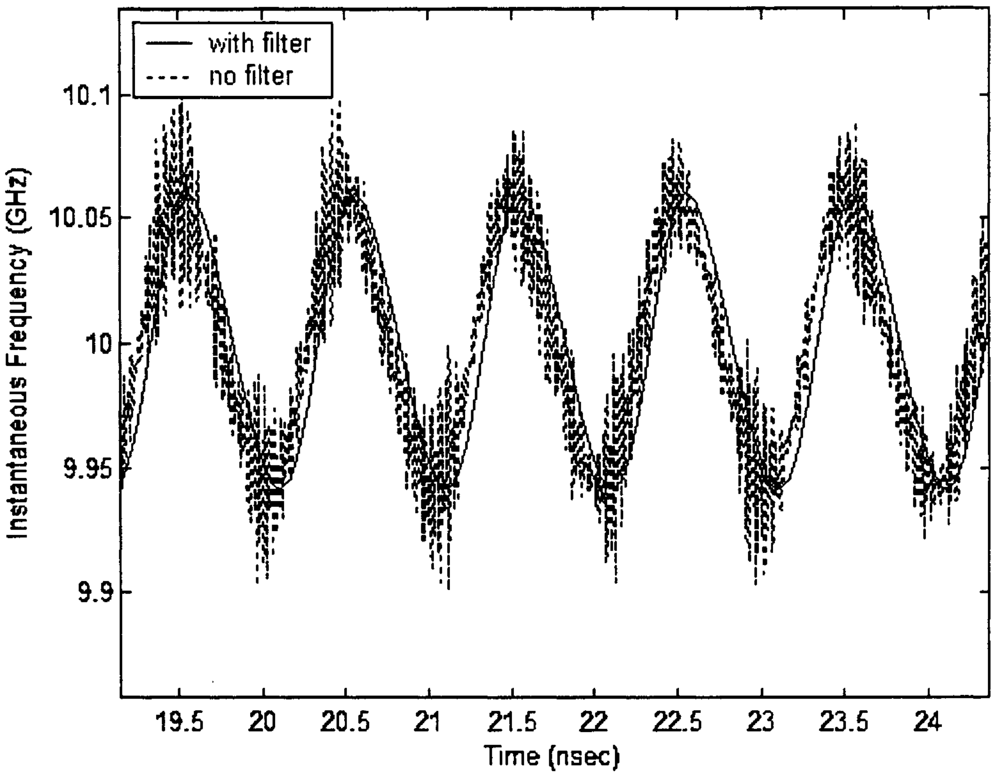

Figure 3.16 Comparison of Instantaneous Frequency Calculated Using FDTD simulation between with filter and no filter Design for the Null Length Slab

3.7 VERSATILITY OF THE FDTD APPROACH OVER ANALYTICAL TECHNIQUES

In previous sections we assumed a permittivity variation of the form (3-2). This enabled us to benchmark the FDTD predictions against approximate analytical solutions available for such a variation. However, since we are able to select a fairly arbitrary functional form for $\varepsilon_r(t)$ using the "table-look-up" scheme we devised in Section 3.3, we will be able to model situations not possible with the analysis of [1]. For instance, consider the case where the permittivity has a time dependence in the form of a square wave of period T_p and modulation depth b as sketched in Figure 3.16.

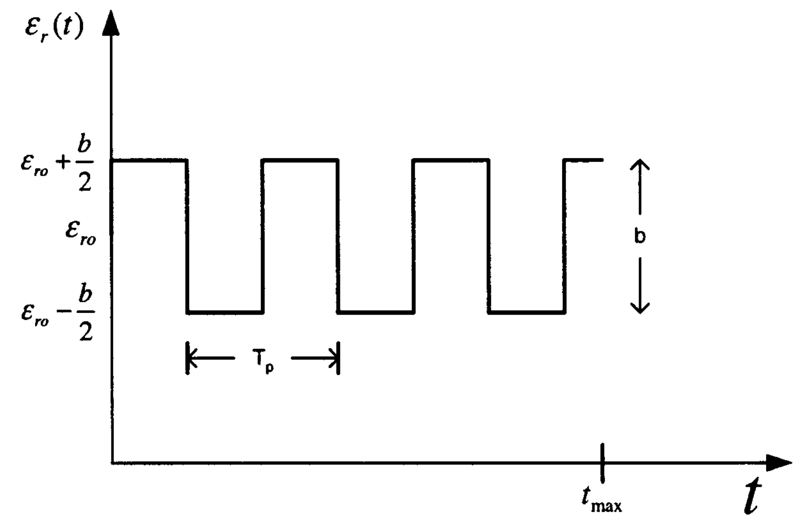

Figure 3.17 Square Wave Permittivity Modulation

The results of the FDTD simulation are shown in Figure 3.18. These show an expected frequency change, but appear to be "noisy". However, the reason (and the ability of the FDTD method to predict what we might not expect, but what is nevertheless correct) can be seen by further examining the form of the permittivity variation. The time-dependence shown in Figure 3.17 can be represented by the Fourier series

$$\varepsilon_r(t) = \varepsilon_{ro} + \frac{b}{2}\left[\frac{4}{\pi}\sum_{n=1,3,5,...}^{N}\frac{1}{n}\sin\left(\frac{2n\pi t}{T_p}\right)\right] \tag{3-26}$$

In order to obtain an "exact" representation we need to have $N \rightarrow \infty$. However, the FDTD will not resolve any components of this variation higher than 100 GHz. The implication can be appreciated if we plot (3-26) with N = 49, since that will remove all Fourier harmonics larger 100 GHz. The graph of this truncated Fourier series is shown in Figure 3.19, where we see that the modulation effectively "rings", resulting in the rapid frequency variation in Figure 3.18.

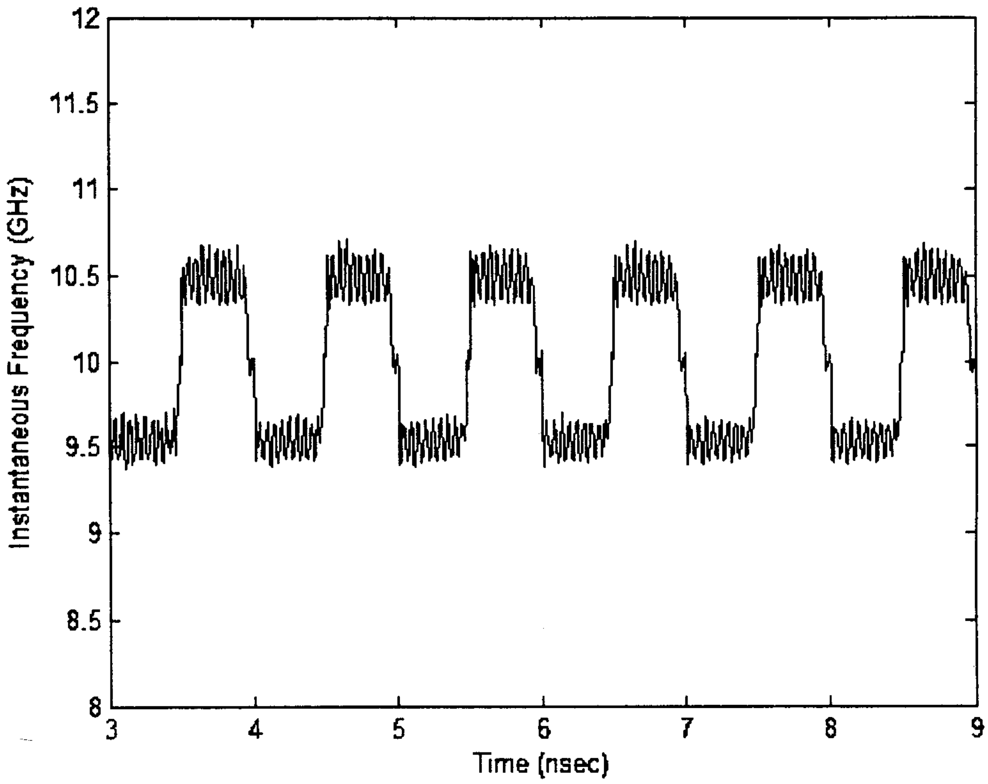

Figure 3.18 FDTD-Predicted Instantaneous Frequency (——) Obtained Using the Electric Field $E_z(x_o,t)$ Observed at $x_o = x_{out} + 2\Delta x$. The Modulation Had a Square-Wave Time-Dependence With A Modulation Depth b = 0.2.

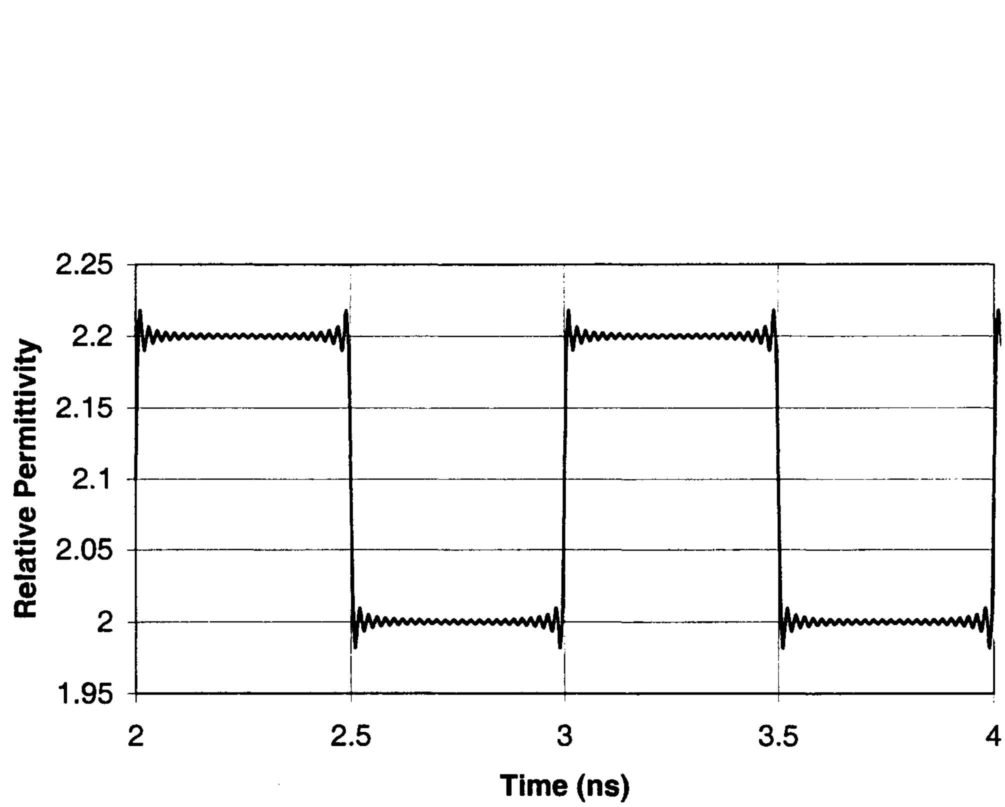

Figure 3.19 Permittivity of Dielectric Slab as Revealed by the Truncated Fourier Series Representation of Figure 3.17

3.8 CONCLUSIONS

In this chapter we explored the use of the FDTD method in modeling the problem of an electromagnetic plane wave incident on a dielectric slab of fixed thickness whose permittivity is independently time-varying. This problem could be classified as one for which we have "electromagnetic wave *propagation through* a time-varying medium", and does not appear to have received attention elsewhere in this precise form using time-domain numerical modelling. We validated the FDTD results through comparison with existing approximate analytical solutions when the material permittivity is sinusoidally time-varying. We found that the two approaches gave identical results for the restricted range of parameters over which the said analytical solutions are valid. However, the FDTD method was shown to be more versatile in that it is not restricted to the above-mentioned range of parameters, nor to only sinusoidal permittivity time-dependences. The examples were presented in such a way that the potential usefulness of the FDTD approach in studying the behaviour of future devices made of distributed time-varying material was apparent.

3.7 REFERENCES FOR CHAPTER 3

[1] F. R. Morgenthaler,"Velocity Modulation of Electromagnetic Waves," *IRE Trans. Microwave Theory Tech.*, vol. 6, pp. 167-172, Apr. 1958.

[2] A.Taflove & S.C.Hagness, "Computational Electrodynamics : The Finite-Difference Time-Domain Method" (Artech House Inc., 2000) 2nd Edition.

[3] D.G.Dudley, "Mathematical Foundations for Electromagnetic Theory" (IEEE Press, 1994).

[4] B.Boashash, "Estimating and interpreting the instantaneous frequency of a signal – Part 2 : Algorithms and applications", Proc. IEEE, Vol.80, No.4, pp.540-568, April 1992.

[5] The *MATLAB* package of The MathWorks, Inc., USA.

[6] M.R.Zunoubi, K.C.Donepudi, J.Jin & W.C.Chew, "Efficient time-domain and frequency-domain finite-element solution of Maxwell's equations using spectral Lanczos decomposition method", IEEE Trans. Microwave Theory Tech., Vol.46, No.8, pp.1141-1149, Aug.1998.

[7] The *MATLAB* routines *buttord, butter, freqz* and *filter* have been used. The *MATLAB* package is a product of The MathWorks, Inc., USA.

[8] A.Zhao and V. Raisanen, " Application of a simple and efficient source excitation technique to the FDTD analysis of wave guide and microstrip circuits," *IEEE Trans. Mcirowave Theory Tech.*, vol. 44, pp. 1535-1539, Sept.1996.

CHAPTER 4

FDTD Analysis of a Microstrip Transmission Line with a Substrate of Independently Time-varying Permittivity

4.1 INTRODUCTION

The previous chapter considered the idealized one-dimensional scalar problem of electromagnetic plane wave interaction with an infinitely large dielectric slab of finite thickness. This is a useful problem since it lends itself to an approximate closed-form analysis considered earlier by several authors. It was thus possible to validate the FDTD approach through reference to such closed-form results.

In this chapter we apply a fully three-dimensional FDTD method to the problem of electromagnetic wave propagation on a microstrip line whose substrate has an independently time-varying permittivity. This does not lend itself to closed-form analysis and, as far as we have been able to establish, its study has not been reported elsewhere in the literature. Yet it is essential that we be able to establish whether the computed performance we obtain using the FDTD approach is meaningful or not. Thus we have adopted the following avenue of investigation :

- We first simply use the FDTD to simulate the microstrip line with a constant value of substrate permittivity (i.e no variation with time). By doing a thorough examination of the various forms of output we will be able to better interpret the more complicated results that will be obtained in later sections when the properties do indeed vary with time.

- We then simulate the microstrip line when it has a time-varying permittivity.

4.2 THE MICROSTRIP LINE GEOMETRY

Figure 4.1 shows the microstrip line that we are interested in. It is of length L and has a dielectric substrate of height H and relative permittivity ε_r, and the conducting track width is W.

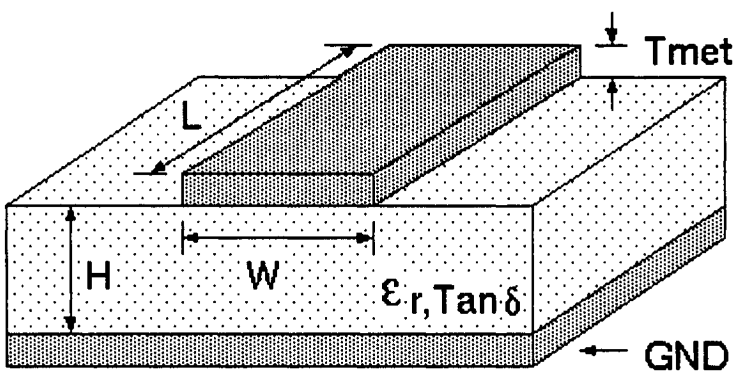

Figure 4.1 Geometry of the Microstrip Line

4.3 IMPLEMENTATION OF THE FULLY THREE-DIMENSIONAL FDTD METHOD USED

Although the FDTD algorithm is relatively easy to code, we have used portions of the FDTD code *QFDTD90* [2] in this work. Unlike most commercially available codes, this one is available in source code format. It was therefore possible to make alterations in order to be able to incorporate materials with independently time-varying properties in the code. The code implements the FDTD algorithm provided in Section 2.3.3. It applies the boundary conditions of Section 2.3.5. Thus it can model three dimensional structures with arbitrary dielectric materials and arbitrary metal structures. The ABC used is the Mur second-order one described in Appendix I. In this work we have incorporated a time-varying material capability and the use of an FFT algorithm to obtain the spectrum of the output time-domain signal.

In the next section we will perform an FDTD simulation of a straight section of microstrip line. The coordinate axes are aligned so that the line is parallel to the z-axis, the point y = 0 falls at the cross-sectional center of the conducting track, and x = 0 at the groundplane. This is shown in Figure 4.2.

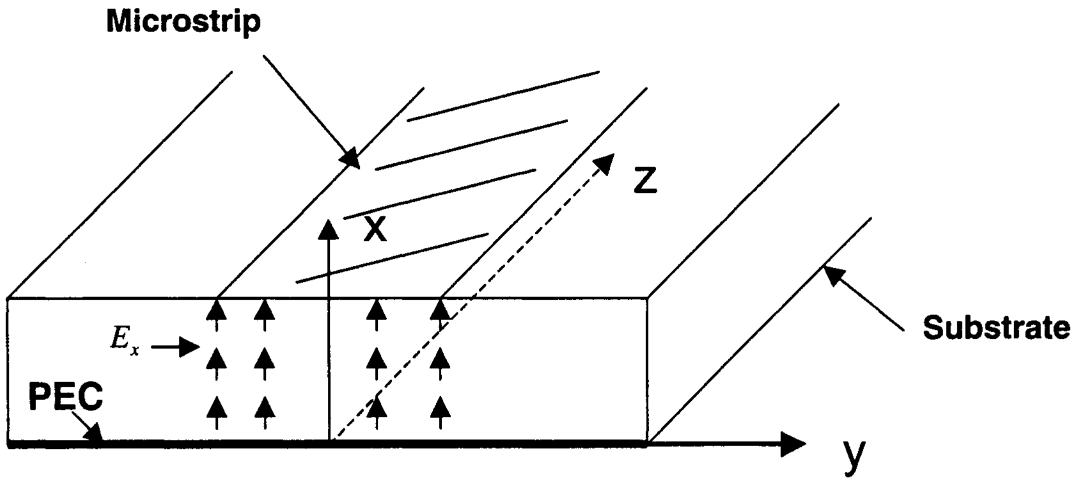

Figure 4.2 Coordinate System for FDTD Model of the Microstrip Line

The simulation structure is backed by a ground plane in the bottom and terminated with ABCs on the other five outer boundaries. The ABC on the input side is at z = 0. The excitation source is applied a few cells inside this ABC . The dominant electric field component in the region between the conducting track and the groundplane is $E_x(x,y,z,t)$. It is convenient to "measure" the electromagnetic field between the conducting track and the groundplane by computing a voltage

$$V(z,t) = -\int_0^H E_x(x, y = 0, z, t)dx \tag{4-1}$$

In this chapter, when we refer to the FDTD "signal", it is this *V(z,t)* that is being referred to.

4.4 FDTD SIMULATION OF THE MICROSTRIP LINE WITH CONSTANT SUBSTRATE PERMITTIVITY

We first keep the substrate permittivity constant, and excite the patch with a source of frequency f_s = 10 GHz. The finite-duration causal sinusoidal source of Section 2.4.2 is used. We then know that for sufficiently large duration t_{max} the spectrum of this signal should be dominated by a spectral line at frequency f_s.

The microstrip line selected was one with H = 0.5 mm, W = 0.5 mm and conductor thickness T_{met} = 0.0 mm. The relative permittivity of the substrate has a value ε_{ro} = 9.6. The FDTD model has Yee cell dimensions $\Delta x = \Delta y = \Delta z$ = 0.125 mm. Finally the time-step Δt must be selected to satisfy the stability criterion of Section 2.3.4; we have used Δt = 0.241 ps. The above-mentioned cell sizes and time step are used throughout this chapter. It will be convenient to write $t_{max} = N_{step}\,\Delta t$, where N_{step} is the number of time-steps for which the FDTD algorithm is allowed to run.

Figure 4.3 shows the analytical Fourier transform of the finite-duration causal sinusoidal source, obtained using expression (2-21) with f_s = 10 GHz and t_{max} = 3.856 ns). Figure 4.4 shows the spectrum of the FDTD signal at a point z_{input} = 1.25mm near the source and z_{output} = 77.5mm at the end of the microstrip line when L = 77.5 mm for N_{step} = 16000 (so that t_{max} = 3.856 ns). It is clear that these match those predicted analytically, and that the FDTD model is properly set up in the sense that no additional significant spectral components are non-physically generated by the FDTD simulation on the constant permittivity substrate. It also confirms that that our FFT implementation correctly transforms the time-domain data to the frequency domain.

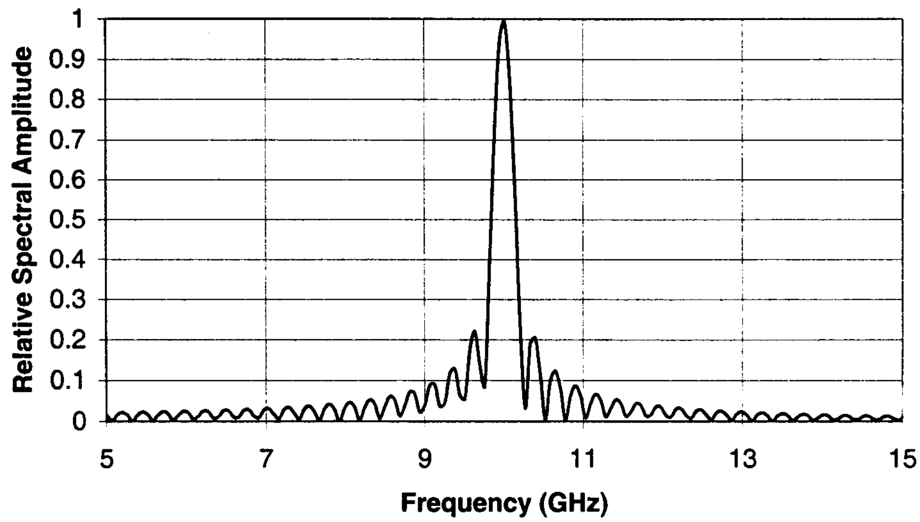

Figure 4.3 Analytical Spectrum of the Finite-Duration Causal Sinusoidal Source with f_s = 10 GHz and t_{max} = 3.856ns.

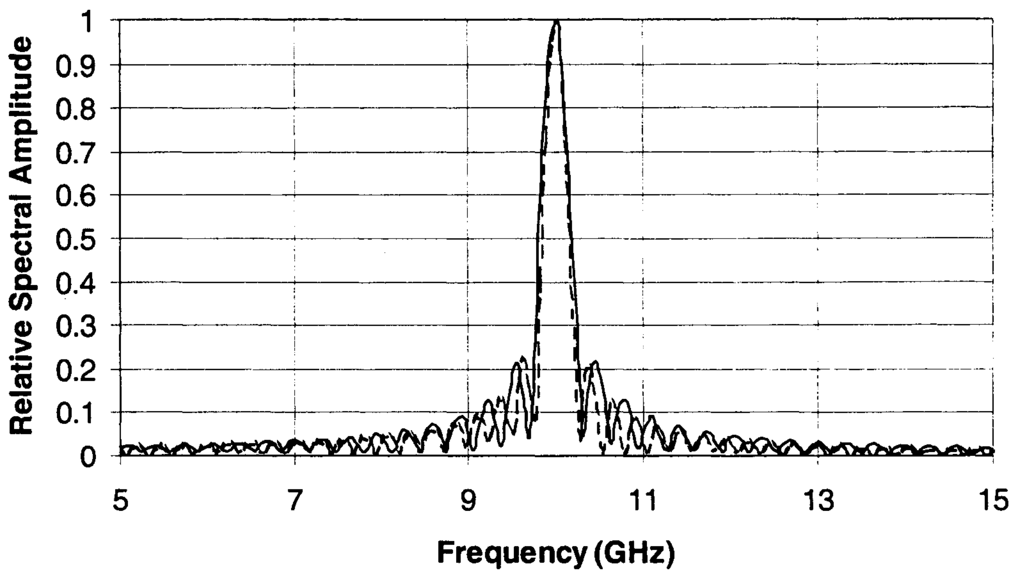

Figure 4.4 Spectrum of the FDTD-Computed Signal at Position z_{input} = 10Δz =1.25mm (- - - -) and z_{output} = 620Δz = 77.5 mm (——) on the Microstrip Line for a Finite-Duration Causal Sinusoidal Source with f_s = 10 GHz and t_{max} = 3.856 ns.

As a further validation of the FDTD model of the microstrip line we wish to examine the signal velocity. We can use a well-known approximate analytical expression [2] to predict the phase velocity of propagation on a microstrip line as

$$v_p = \frac{c}{\sqrt{\varepsilon_{eff}}} \tag{4-2}$$

where the effective relative permittivity ε_{eff} is

$$\varepsilon_{eff} = \frac{\varepsilon_r + 1}{2} + \frac{\varepsilon_r - 1}{2} \cdot \frac{1}{\sqrt{1 + 12 \cdot \frac{H}{W}}} \tag{4-3}$$

In the case of the microstrip line dimensions being used in this chapter expression (4-3) gives ε_{eff} = 6.4926 and hence a phase velocity of v_p = 1.177 x 10^8 m/s.

We next apply the FDTD method with a causal sinusoidal source of frequency 10GHz, and observe microstrip voltage at 8 locations on the microstrip line. By "tracking" the same point on the wave we can easily determine how long the signal takes to reach these positions. Using this information the phase velocity is computed to be v_p = 1.154 x 10^8 m/s, which is close to the value obtained using the above-mentioned approximate expression.

4.5 FDTD SIMULATION OF THE MICROSTRIP LINE WITH INDEPENDENTLY TIME-VARYING SUBSTRATE PERMITTIVITY

In this section we consider the same microstrip line used in Section 4.4, except that now the substrate permittivity is allowed to vary as

$$\varepsilon\,(t) = \varepsilon_0 \varepsilon_{r0}(1 + b\sin\omega_m t) = \varepsilon_0\, \varepsilon_r(t) \tag{4-4}$$

The FDTD model has same Yee cell dimensions Δx = Δy = Δz = 0.125 mm, and which are small enough size to handle highest frequency up to 30GHz. Since ε_{ro} = 9.6 and b = 0.4792, the maximum value reached by the relative permittivity is $\varepsilon_r^{MAX} = 14.2$. Even as high as 30GHz the wavelength in this media is thus $\lambda_e = \lambda_0 / \sqrt{\varepsilon_r^{MAX}}$ = 2.65mm, and thus for all frequencies the spatial step is less than the $\lambda_e/20$.

Although the use of a section of microstrip line such as that being considered here has been suggested for use as an adjustable phase shifter [5], in which the substrate permittivity is controllable, such applications (as mentioned in Chapter 1) are using the permittivity change to reconfigure the device. The change in permittivity in [5] is at a rate orders of magnitude lower than that of the electromagnetic wave's source frequency f_s passing through the device. Thus their device is not a frequency changer in any way. Here we wish to examine what happens to the signal spectrum when the permittivity change is rapid.

It is of course necessary to select specific numerical values for several parameters. As in Section 4.4 we use $f_s = 10$ GHz and $t_{max} = 3.856$ns (obtained by using $N_{step} = 16000$). Furthermore, in the results to be demonstrated we have used $f_m = 3$ GHz and a line length z = 77.5mm. As described in Section 4.3, the FDTD simulation provides $V(z,t)$. Since the output in this case of time-varying permittivity will depend on the value of the modulation index b we will for clarity and notational convenience henceforth write the output as $V(b,z,t)$. We will often examine the spectrum of this output and so will write the Fourier transform of this quantity with respect to time as $F(b,z,f) = FFT\{V(b,z,t)\}$, where f is the frequency the "FFT" indicates that a fast Fourier transform algorithm has been used on the FDTD computed data. In displaying and interpreting the computed data we will usually fix two of the parameters and use the third as the independent variable in the plot.

Figure 4.5 shows $F(b,z,f)$ as a function of frequency for $b = 0.4792$ at two different values of z. We observe that there are other spectral components in addition to that at the source frequency f_s, and that the relative amplitudes of spectral components depend on the location (that is, value of z) on the microstrip line at which the spectrum is observed. The dominant additional frequencies are indeed at $f_s \pm nf_m$ (n an integer) as expected when "mixing" occurs due to the sinusoidal time-variation of the substrate permittivity. While this result may be considered to be precisely "what was expected" we note that this is, to the present author's knowledge, the first time this has actually been demonstrated using an FDTD formulation with time-varying permittivity, and certainly for a practical structure such a microstrip line.

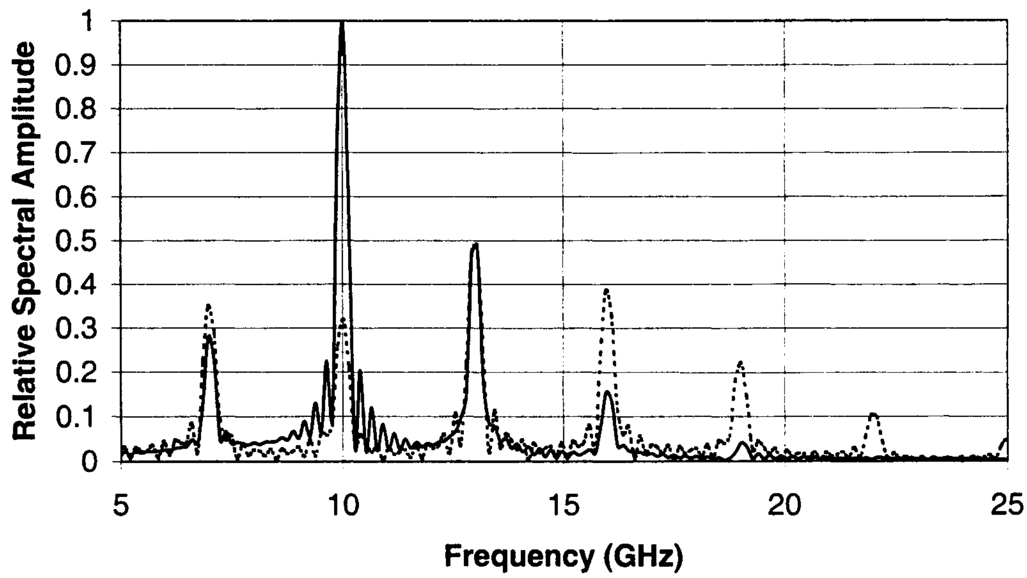

Figure 4.5 The Spectrum *F(b,z,f)* as a Function of Frequency at Two Different Values of z. These Values are z = 45Δz = 5.625mm (——) and z = 145Δz = 18.125mm (- - - -). The Modulation Index is 0.4792.

The dependence of the spectral composition on position prompts us to examine $F(b,z,f_p)$ as a function of z for selected values of f_p. In other words, we will examine the amplitudes of selected spectral components. These are shown in Figure 4.6 for f_p = 7GHz, 10 GHz, 13 GHz, 16 GHz. Observe that these are apparently a periodic function of position. At particular positions the mixed frequencies have a larger amplitude than the signal frequency.

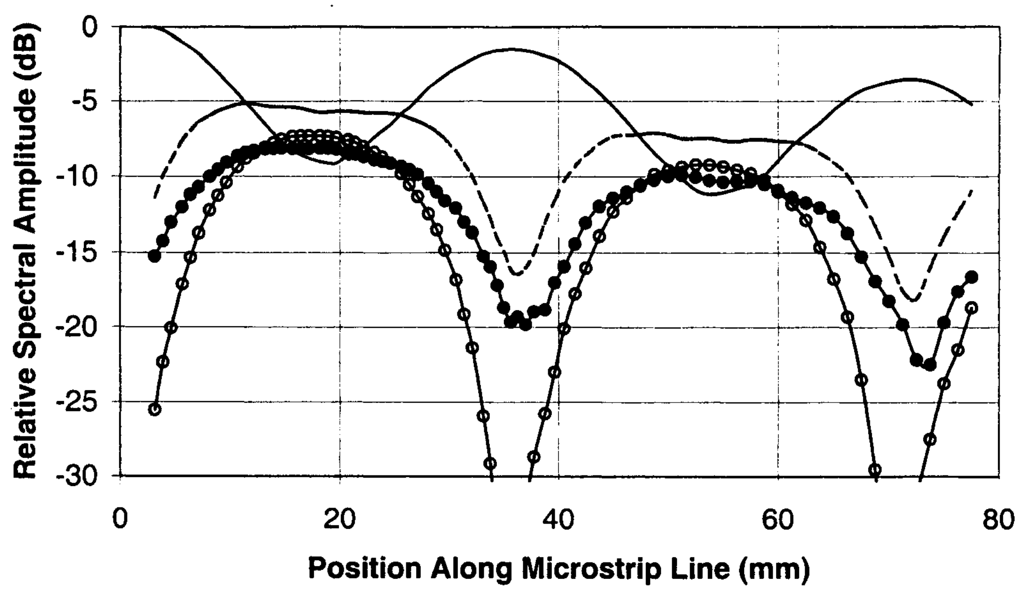

Figure 4.6 The Spectrum $F(b,z,f_p)$ as a Function of z for Selected Values of f_p = 7GHz (- - - -), 10 GHz (——), 13 GHz (●-●-●-●) and 16 GHz (o-o-o-o). All Quantities are Normalised to the 10GHz Spectral Amplitude at z = 25Δz = 3.125mm.

We would expect the amplitudes of the mixed frequencies to (as a trend) exhibit an increase as the modulation depth b increases. Figure 4.7 show $F(b,z,f_p)$ as a function of b at position z = 45Δz = 5.625mm. Observe that the amplitude of the source frequency component decreases as the others increase when b becomes larger. The results shown are of course exhibited at other positions, although the relative spectral amplitudes are different, which is to be expected from the observations made in Figure 4.5. The results shown here are for a microstrip line of length L = 10mm, but similar behaviour is predicted for other line lengths.

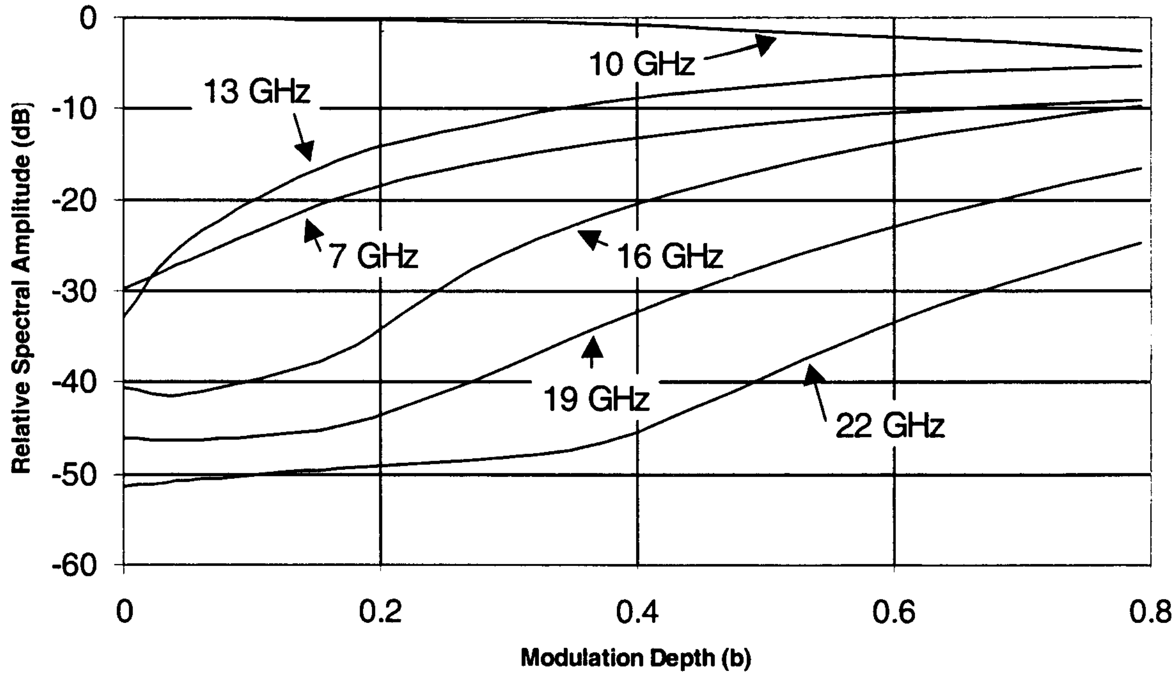

Figure 4.7 The Spectrum $F(b,z,f_p)$ as a Function of Modulation Depth b at Position z = 45Δz = 5.625mm for Selected Values of f_p

4.6 CONCLUDING REMARKS

In this chapter we explored the use of the FDTD method in modeling the problem of an electromagnetic wave propagating along a section of microstrip line of fixed width and substrate height, but whose substrate permittivity is independently time-varying. This problem could be classified as one for which we have an "electromagnetic wave *propagation along* a time-varying medium". As far as we have been able to establish, neither this specific problem nor something in this class of problem has received attention in the literature.

We ensured that we had a proper understanding of how to interpret the FDTD results by first keeping the substrate permittivity constant and examining the field spectra. We also ensured that the FDTD model of the microstrip line was correct by comparing the FDTD phase-velocity prediction (for the constant permittivity case) to well-known approximate closed-form expressions. Only then did we proceed to the time-varying substrate situation.

We then examined the FDTD-computed results for the time-varying substrate permittivity case and were able to interpret the presence and variation of the "mixed" frequency components. This example is close to what might be in real-world future devices made of distributed time-varying material.

4.7 REFERENCES FOR CHAPTER 4

[1] D.M. Pozar, "*Microwave Engineering,*" 2nd edition, Wiley, 1998.

[2] Y. Qian and T. Itoh, *FDTD Analysis and Design of Microwave Circuits and Antennas* (Realize Inc.,1999).

[3] The *MATLAB* package of The MathWorks, Inc., USA.

[4] I. J. Bahl and R.Garg, "Simple and Accurate Formulas for Microstrip with Finite Strip Thickness" Proc. *IEEE*, Vol. 65, pp. 1611-1612, 1977.

[5] F. de Flaviis, N.G.Alexopoulos & O.M.Stafsudd, "Planar microwave integrated phase-shifter design with high purity ferroelectric material", IEEE Trans. Microwave Theory Tech., Vol.MTT-45, No.6, pp.963-969, June 1997.

[] D. E. Holberg and K. S. Kunz, "Parametric Properties of Fields in a Slab of Time-Varying Permittivity," *IEEE Trans. Antennas Propagat.*, vol. 14, pp. 183-194, March 1966.

CHAPTER 5

FDTD Analysis of a Microstrip Antenna on a Substrate of Independently Time-Varying Permittivity

5.1 INTRODUCTION

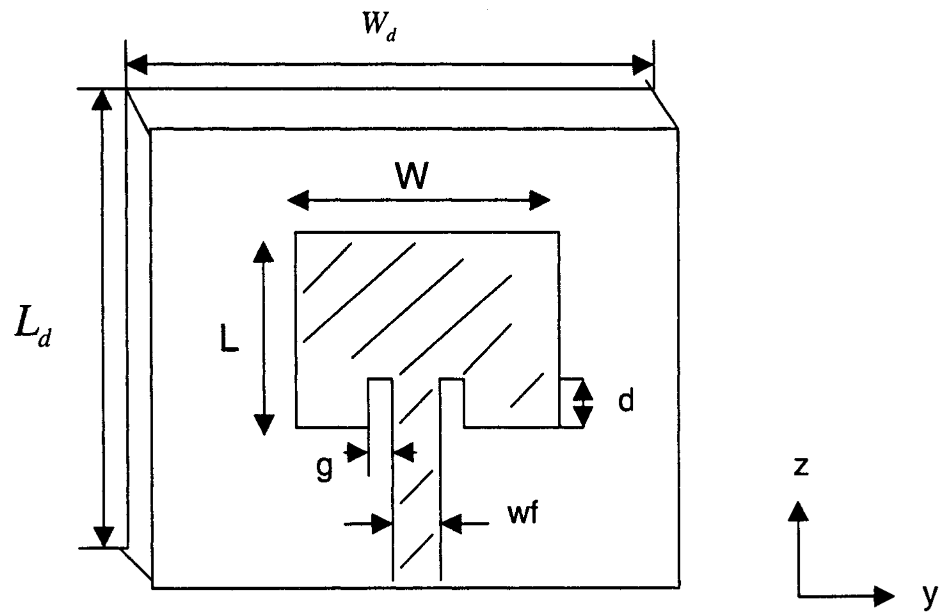

Figure 5.1 Inset Fed Microstrip Patch Antenna

A microstrip patch antenna with an inset in the feedline is shown in Figure 5.1 [1]. The coordinate system orientation used in the analysis is also shown. The x-axis is perpendicular to the plane of the conducting patch, and the feedline is parallel to the z-axis. Thus the radiation pattern of the antenna in the xz-plane (that is, $\phi = 0°$ and varying

θ) is the E-plane pattern of the antenna. The xy-plane (that is, $\theta = 90°$ and varying ϕ) is the H-plane pattern of the antenna. Since the emphasis in this thesis is not specifically on the design aspects of microstrip patch antennas, we have selected a design whose details are available in the literature and whose center-frequency is 5.8GHz. The relative permittivity of the substrate is $\varepsilon_r = 2.33$, the length of the patch is L = 16.3mm, the width W = 25.15mm, feedline width $W_f = 2.286$mm, inset depth d = 3.668mm, and inset gap width g = 0.762mm. The finite substrate (and hence groundplane) width is W_d = 40.386mm and length L_d = 32.6mm. These dimensions will be used throughout this chapter. It is only the ε_r that will be made to vary with time. We use the same FDTD code as in Chapter 4, except that here it is applied to the antenna radiation problem.

In Section 5.2 we will briefly describe how the far-zone radiation patterns of the antenna can be computed using an FDTD model. We will in Section 5.3 carefully examine the FDTD results for the antenna when the permittivity of the substrate is kept constant. This is essential in order to be able to properly interpret the simulation results when the permittivity is allowed to vary. Section 5.4 considers the independently time-varying permittivity case. Section 5.5 concludes the chapter.

5.2 NEAR-FIELD TO FAR-FIELD TRANSFORMATION SCHEME FOR *FDTD* METHOD

Several schemes for determining far-zone radiation patterns from FDTD computations have been presented in the literature [2,3]. In this section we will describe the method used to obtain the antenna radiation patterns that will be shown in Sections 5.3 and 5.4. As noted in Section 2.3, the FDTD grid must be truncated on a surface surrounding the structure being analysed using some form of radiation boundary condition. Thus for the antenna in Figure 5.1 we will have such a "truncation surface" (say $S_{truncate}$) completely surrounding the antenna at some finite distance away from the antenna. We can then consider another surface (say S_{eq}) that also completely surrounds the antenna in question, but which lies within $S_{truncate}$ (eg. 3 to 4 cells inside the FDTD "ABC box").. Suppose we wish to compute the far-zone radiation pattern of the antenna at some frequency $\omega_p = 2\pi f_p$. The FDTD method is then allowed to run for a suitable value of t_{max} so that a steady-state is reached. The FDTD-computed electric and magnetic fields are determined at points on S_{eq} at frequency ω_p using a "running DFT" as the FDTD algorithm runs up to time t_{max}. These fields are then used to determine equivalent current densities on S_{eq} according to the surface equivalence theorem [4], and these current densities are used in the radiation integrals [4] to determine the far-zone fields $E_\theta(\theta,\phi)$ and $E_\phi(\theta,\phi)$ in directions direction (θ,ϕ) at frequency ω_p.

5.3 PREDICTED PERFORMANCE OF THE MICROSTRIP PATCH ANTENNA ON A SUBSTRATE WITH CONSTANT PERMITTIVITY

As a first check on the FDTD modeling of the patch antenna we will use a Gaussian pulse as input so as to be able to obtain the input return loss of the antenna over a broad range of frequencies. Using an FDTD cell size of $\Delta x = 0.2625$mm, $\Delta y = 0.762$mm and $\Delta z = 0.4075$mm, a value $\Delta t = 7.0705 \times 10^{-4}$ ns, and a Gaussian pulse of width $t_w = 30$ps, we obtain the return loss (RL) shown in Figure 5.2. This is determined from the FDTD-computed voltages as

$$RL(f) = 20\log_{10}\left[\frac{FFT\{V_{refl}(z_{port},t)\}}{FFT\{V_{inc}(z_{port},t)\}}\right] \tag{5-1}$$

where $V_{refl}(z_{port},t)$ is the reflected voltage at this port, and $V_{inc}(z_{port},t)$ is the incident voltage at this port. Also shown is the return loss computed using the frequency-domain moment method based commercial code *IE3D* [5]. The relatively good agreement provides verification of the FDTD model.

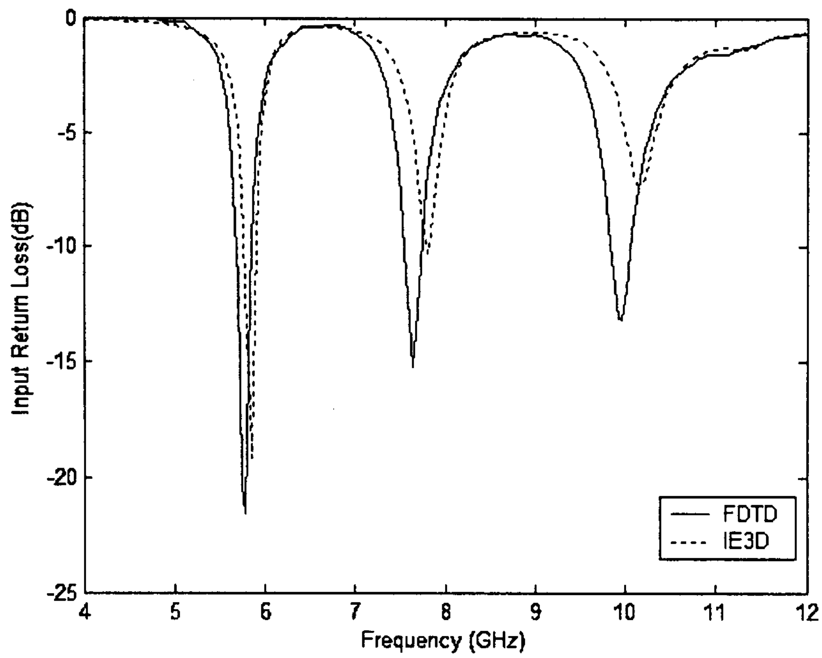

Figure 5.2 Simulated Results of the Input Return Loss of the Patch Antenna Using FDTD and IE3D Simulation

When we consider the case of time-varying substrate permittivity in Section 5.4, we will wish to use a sinusoidally time-varying source to drive the FDTD simulation, for the same reasons as in Chapter 4. We will use the center-frequency of the antenna as the source frequency, namely $f_s = 5.8$ GHz. The length of a time step is $\Delta t = 7.0705 \times 10^{-4}$ ns as before. In the discussion that follows we will examine the results from the FDTD simulation for several durations $t_{max} = t_n$, for n = 1,2,3,4,5,6. The numerical values are shown in Table 5.1. Clearly we have $t_1 < t_2 < t_3 < t_4 < t_5 < t_6$.

Table 5.1 Tabulation of "Elapsed Times" Referenced in the Text ($\Delta t = 7.0705 \times 10^{-4}$ ns)

Elapsed Time (t_{max})	*No. of Time-Steps (N_{step})*	*Value in Nano-Seconds ($N_{step}\ \Delta t$)*
t_1	1000	0.70705
t_2	2000	1.41410
t_3	4000	2.82820
t_4	8000	5.65640
t_5	16000	11.3128
t_6	32000	22.6256

Figure 5.3 shows the computed E-plane far-zone patterns at f_p = 5.8 GHz for the above-mentioned elapsed times. It is clear that for a sufficiently long elapsed time the computed pattern settles down to the steady-state pattern of the antenna at the stated frequency. We have found that for elapsed times larger than t_6 the pattern changes negligibly. Thus in Figure 5.3 we have normalized all the patterns to the maximum value of that for an elapsed time t_6. The H-plane pattern in Figure 5.4 exhibits a similar behaviour.

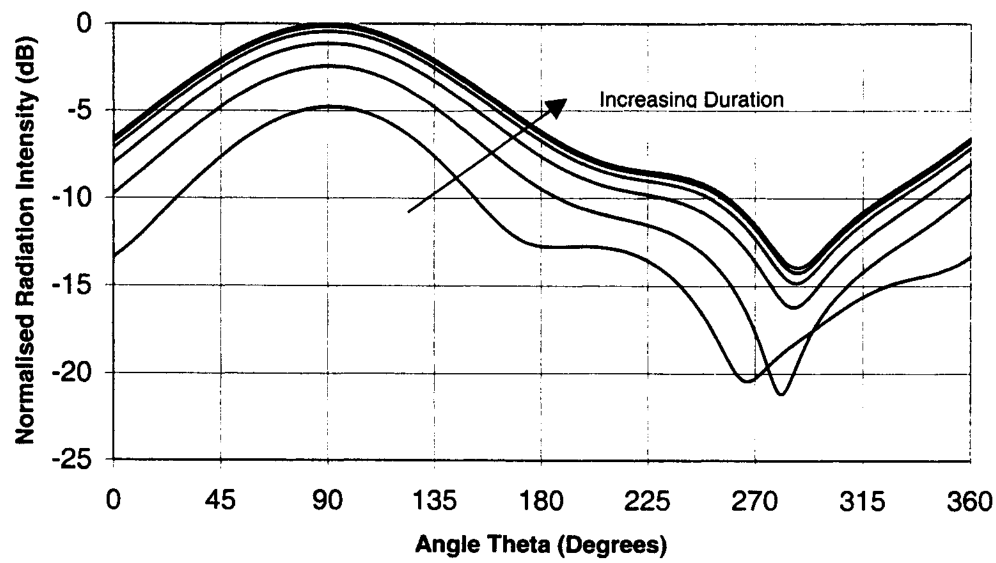

Figure 5.3 **FDTD-Computed E-Plane Normalised Radiation Patterns at 5.8 GHz for Increasing Durations t_{max}. The Source is a Causal Sinusoid of Frequency f_s = 5.8 GHz and Duration t_{max}. The Duration t_{max} Varies from t_1 to t_6 in the Direction Shown.**

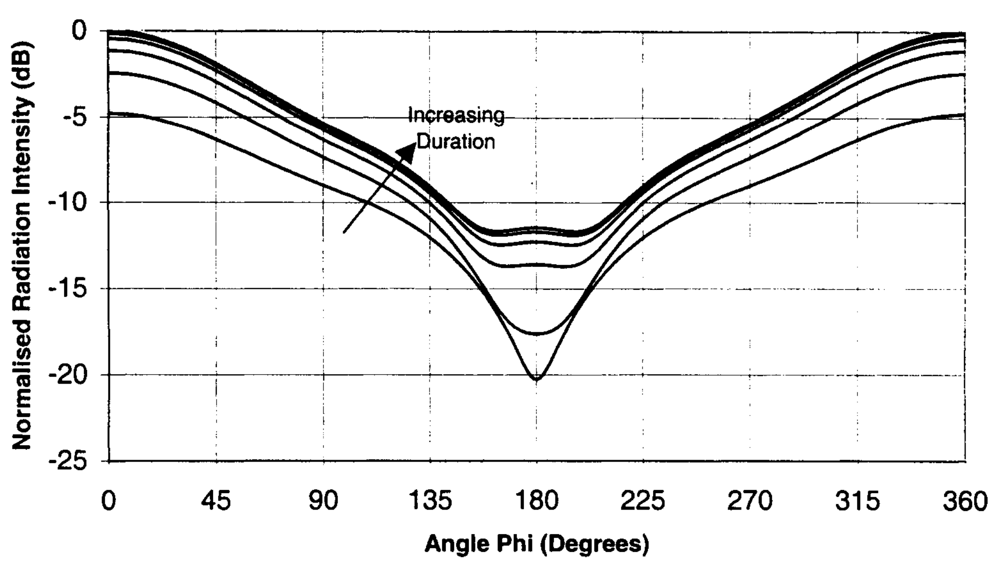

Figure 5.4 **FDTD-Computed H-Plane Normalised Radiation Patterns at 5.8 GHz for Increasing Durations t_{max}. The Source is a Causal Sinusoid of Frequency f_s = 5.8 GHz and Duration t_{max}. The Duration t_{max} Varies from t_1 to t_6 in the Direction Shown.**

The computed radiation E- and H-plane patterns of the antenna at f_p = 7.7 GHz (but still with f_s = 5.8 GHz) are shown in Figures 5.3 and 5.4, respectively. We observe that as the elapsed time increases the compute patterns at this frequency becomes increasingly smaller. This is what we expect. The larger the elapsed time the closer the FDTD results approach the true steady-state values. If the source frequency is for f_s = 5.8 GHz and the antenna parameters are time-invariant then there should be no steady-state radiation patterns at any frequency other than 5.8 GHz. We can compute the radiation pattern level in the direction of the pattern maximum for several frequencies, and plot these in the form of a spectrum shown in Figure 5.7. Observe that this shows that the peak spectral component is indeed at 5.8 GHz. It might appear surprising that there are other frequency components at all, albeit small. However, as discussed in Section 2.4.2, this is simply due to the presence of such frequency components in the causal sinusoidally time-varying source. If we were to use elapsed times very much larger than t_6 we would see that the spectral line at 5.8 GHz becomes sharper.

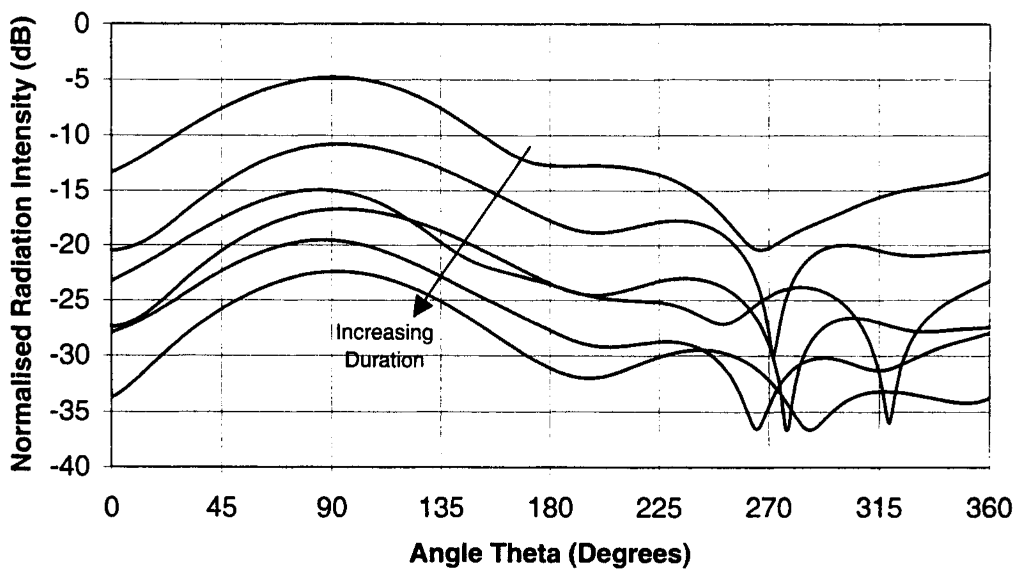

Figure 5.5 FDTD-Computed E-Plane Normalised Radiation Patterns at 7.7 GHz for Increasing Durations t_{max}. The Source is a Causal Sinusoid of Frequency f_s = 5.8 GHz and Duration t_{max}. The Duration t_{max} Varies from t_1 to t_6 in the Direction Shown.

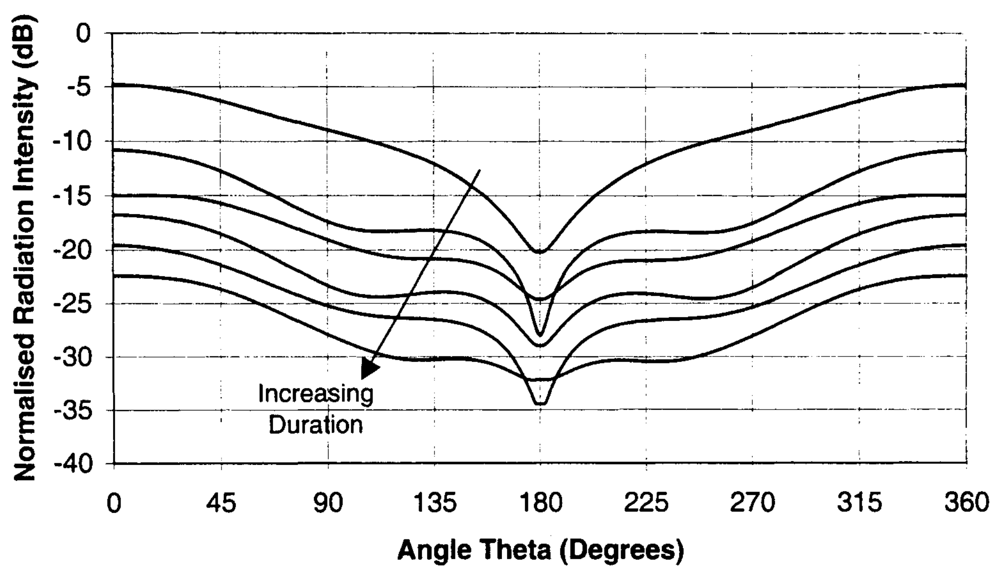

Figure 5.6 FDTD-Computed H-Plane Normalised Radiation Patterns at 7.7 GHz for Increasing Durations t_{max}. The Source is a Causal Sinusoid of Frequency f_s = 5.8 GHz and Duration t_{max}. The Duration t_{max} Varies from t_1 to t_6 in the Direction Shown.

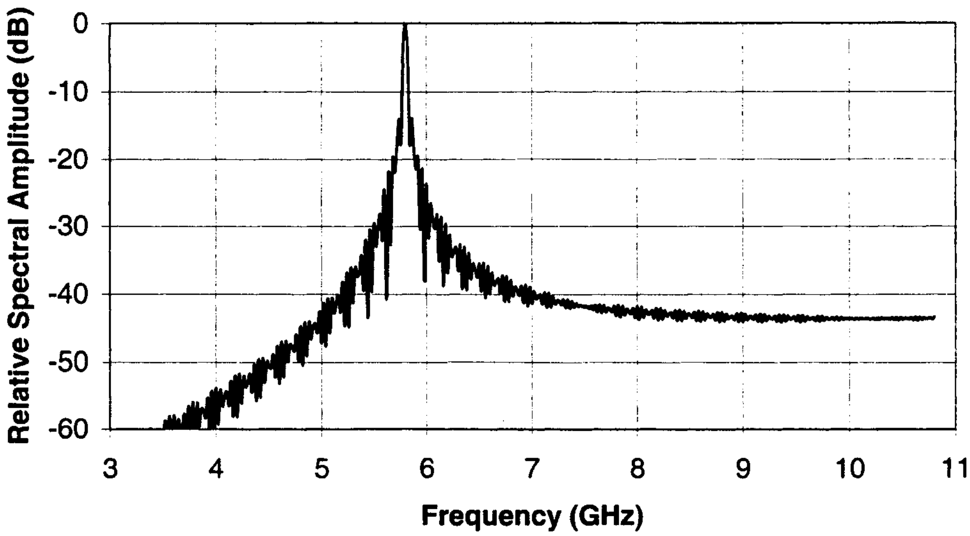

Figure 5.7 FDTD-Computed Spectrum in Direction (θ=0°,φ=0°) for Duration $t_{max} = t_6$. The Source is a Causal Sinusoid of Frequency f_s = 5.8 GHz and Duration t_{max}. There is no Modulation of the Substrate Permittivity.

The results that have been discussed have served to establish the fact that the FDTD simulations correctly describe the transient and steady-state behaviour of the antenna, and have shown how to interpret these to form the correct physical interpretation. Although not an end in itself as far as this thesis is concerned, the in-depth examination of the transient behaviour of a microstrip patch antenna does not appear to have been described by others, and is interesting in its own right. At any rate, we are now ready to proceed to an examination of the far-zone radiation pattern behaviour when the permittivity of the substrate is allowed to vary independently with respect to time.

One final examination of computed radiation patterns with constant substrate permittivity is worth brief consideration. We have computed the radiation patterns of the antenna at 5.8 GHz when using a Gaussian pulse source of width t_w = 30ps and compared it to that with a causal sinusoidal source for an elapsed time $t_{max} = t_4$. These are shown in Figures 5.8 and 5.9. It is clear that even for $t_{max} = t_4$ the patterns have already "settled down" sufficiently, as can also be observed from Figure 5.3.

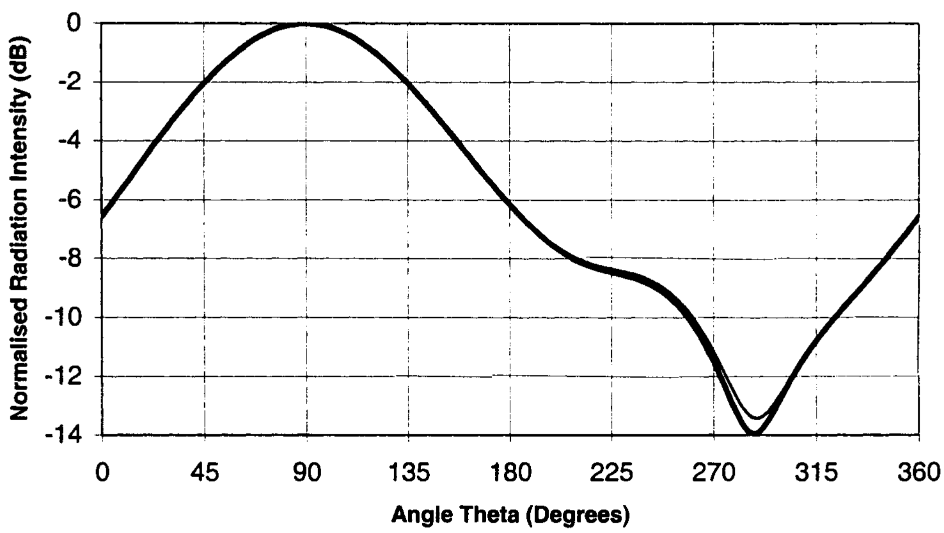

Figure 5.8 Comparison of FDTD-Computed E-Plane Normalised Radiation Patterns at 5.8 GHz Obtained Using a Gaussian Pulse Source (——) and a Causal Sinusoid (▬▬) of Frequency f_s = 5.8 GHz and Duration $t_{max} = t_4$.

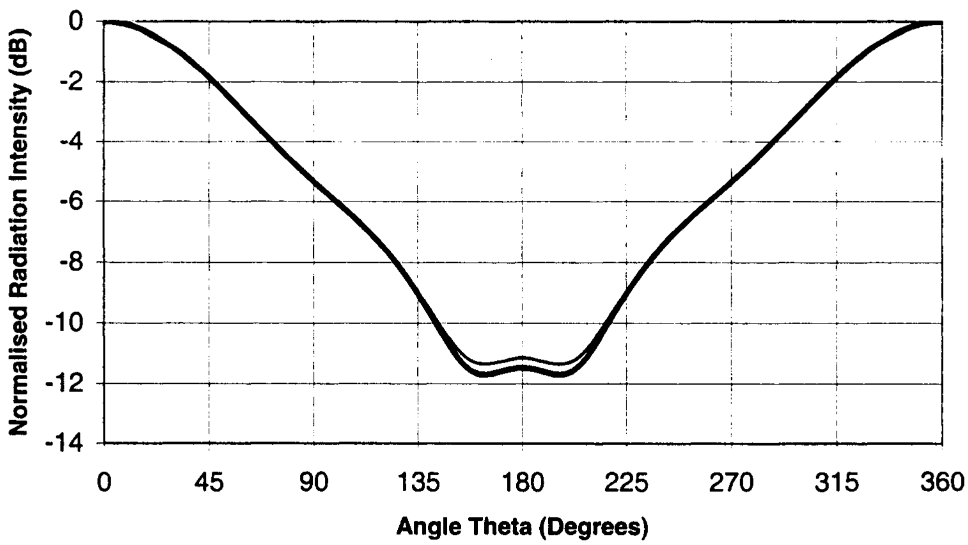

Figure 5.9 Comparison of FDTD-Computed H-Plane Normalised Radiation Patterns at 5.8 GHz Obtained Using a Gaussian Pulse Source (——) and a Causal Sinusoid (▬▬) of Frequency f_s = 5.8 GHz and Duration $t_{max} = t_4$.

5.4 FAR-FIELD PATTERN OF THE PATCH ANTENNA ON A SUBSTRATE WITH TIME-VARYING PERMITTIVITY

In this section we will utilize the FDTD model used in Section 5.3, with a source frequency f_s = 5.8 GHz, but now allow the permittivity of the substrate to vary in time as $\varepsilon(t) = \varepsilon_0 \varepsilon_{r0}(1 + b \sin \omega_m t) = \varepsilon_0 \varepsilon_r(t)$. In particular, we use $\varepsilon_{r0} = 2.33$, $b = 0.429$ and f_m = 2 GHz. The FDTD model has same Yee cell dimensions $\Delta x = \Delta y = \Delta z = 0.125$ mm, and which are small enough size to handle highest frequency up to 30GHz. Since for the problem we have chosen ε_{ro} = 9.6, b=0.4792, then we calculated the maximum of permittivity=14.2, so at 30GHz, the wavelength in this media is $\lambda_e = \lambda_0 / \sqrt{\varepsilon_r^{MAX}}$ =2.65mm. So the spacial step less than the $\lambda_e/20$.

The FDTD-computed spectrum in direction ($\theta = 0°, \phi = 0°$) for duration $t_{max} = t_6$ is shown in Figure 5.10, normalized to the level at the source frequency of 5.8 GHz. There are now radiation patterns of significant levels at frequencies other than just the source frequency f_s. These "mixed frequency" mixed signals appear at frequencies $f_s + nf_m$ (for integer n) as expected. The actual complete radiation patterns of the modulated antenna at selected values of the above-mentioned frequencies are shown in Figures 5.11 and 5.12 for the E-plane and H-plane, respectively.

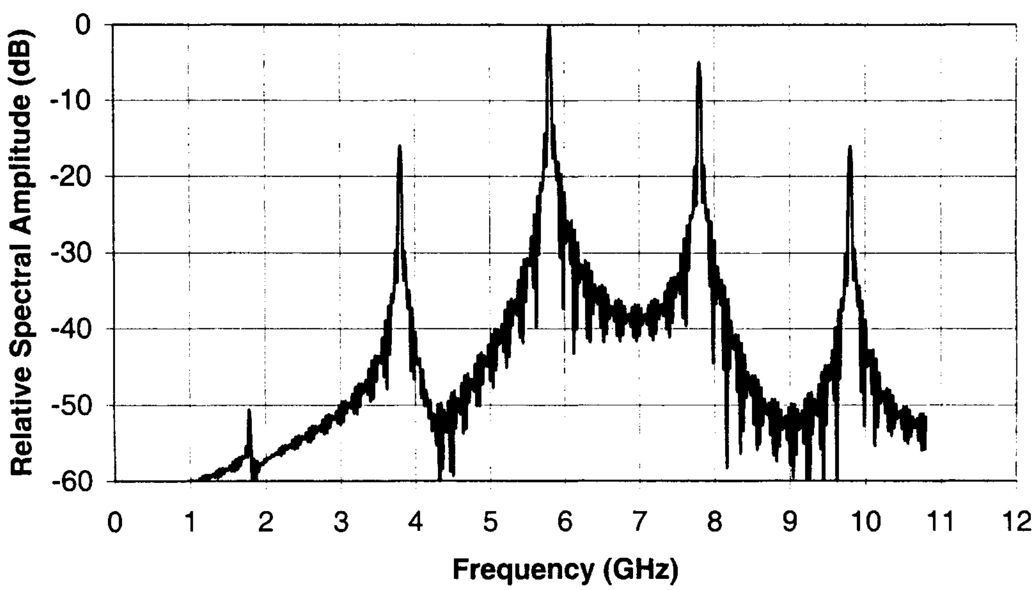

Figure 5.10 FDTD-Computed Spectrum in Direction ($\theta = 0°, \phi = 0°$) for Duration $t_{max} = t_6$. The Source is a Causal Sinusoid of Frequency f_s = 5.8 GHz and Duration t_{max}. The Modulation Frequency is f_m = 2 GHz and Modulation Index b = 0.429.

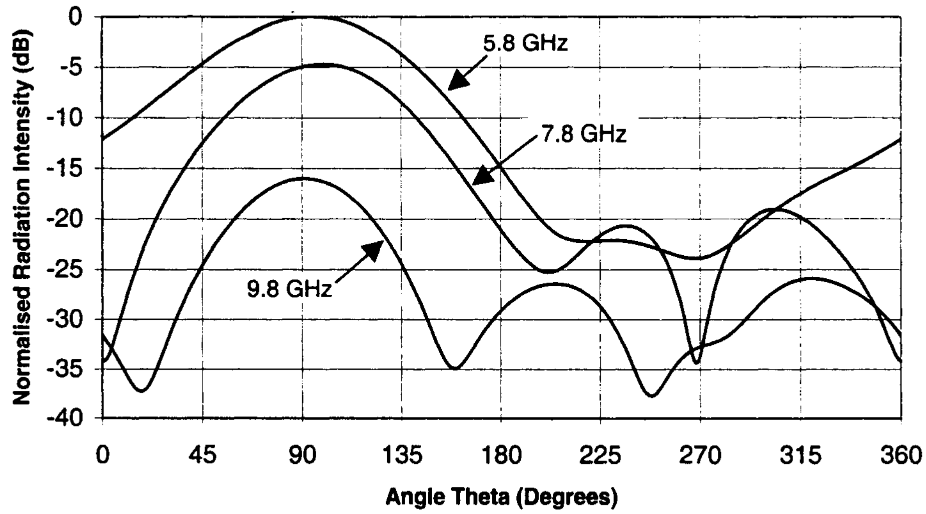

Figure 5.11 **FDTD-Computed E-Plane Radiation Patterns at the Source and Selected Mixed Frequencies for Duration $t_{max} = t_6$. The Source is a Causal Sinusoid of Frequency f_s = 5.8 GHz and Duration t_{max}. The Modulation Frequency is f_m = 2 GHz and Modulation Index b = 0.429.**

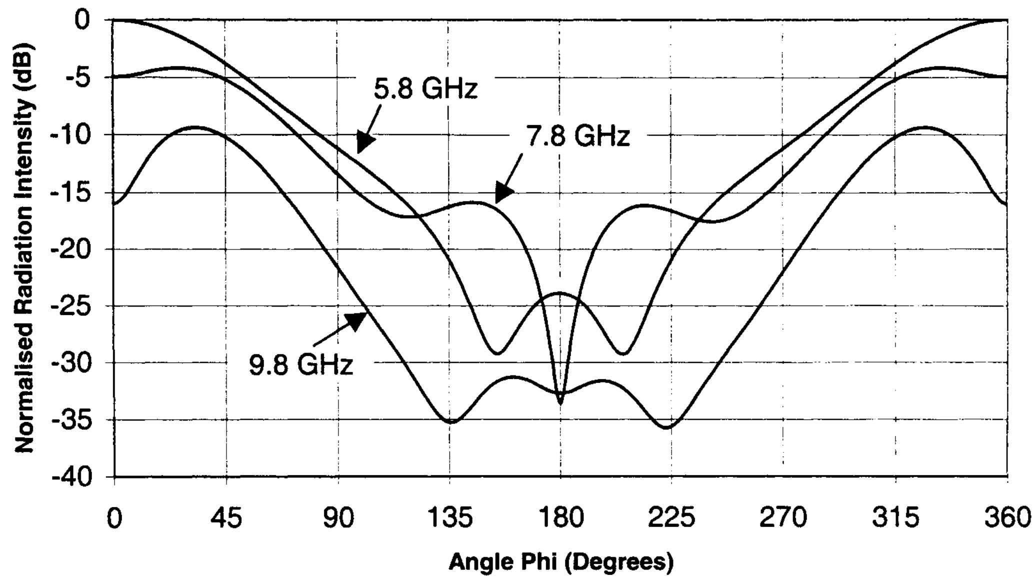

Figure 5.12 **FDTD-Computed H-Plane Radiation Patterns at the Source and Selected Mixed Frequencies for Duration $t_{max} = t_6$. The Source is a Causal Sinusoid of Frequency f_s = 5.8 GHz and Duration t_{max}. The Modulation Frequency is f_m = 2 GHz and Modulation Index b = 0.429.**

Comparing the patterns at 5.8 GHz in Figures 5.11 and 5.12 with those for substrate with constant permittivity in Figures 5.3 and 5.4, we observe that they are not identical. The modulation of the substrate permittivity has not only resulted in radiation at mixed frequencies but in change to the radiation patterns at the source frequency itself. If we examine the relative levels of the radiation patterns at the source frequency (and source amplitudes) for the constant and modulated permittivity cases we observe that that with the substrate modulation present is higher; this phenomenon might be explained in terms of the energy from the physical process that causes the permittivity to vary resulting in some signal ampification.

5.5 CONCLUDING COMMENTS

Radiation from a microstrip patch antenna whose substrate has an independently time-varying permittivity has been considered in this chapter using FDTD modelling. This problem could be classified as one for which we have an "electromagnetic wave *radiation from* a time-varying medium". Once again, as far as we have been able to establish, neither this specific problem nor something in this class of problem has received attention in the literature. We first carefully considered the FDTD output spectrum (and associated radiation patterns) of an antenna with a constant substrate permittivity for increasing values of the time t_{max} for which the input sinusoidal signal is turned on. This enabled us to connect the evolution of the output spectrum of the antenna to the evolution of its radiation patterns at "unwanted" frequencies (i.e. frequencies other than that of the input sinusoid f_s. Armed with this understanding, we then proceeded to the FDTD analysis of the same antenna but with a sinusoidally time-varying substrate. In this situation mixed frequencies are generated and are seen to not "die down" irrespective of how long the time period t_{max} is. By similarly connecting the output spectrum and the radiation patterns at these various mixed frequencies we were able to conclude that the FDTD method is an appropriate simulation tool for modeling the class of problem in question. Although speculative, with appropriate future materials one might envisage antennas that use this approach in order to realize integrated frequency-converters. Until now the use of materials whose permittivity is electronically controllable in antenna designs [6,7,8] has been limited to a role of reconfigurability. The simulations performed here for the first time have demonstrated that future rapidly controllable materials could possibly be used to design antennas with novel properties.

5.6 REFERENCES FOR CHAPTER 5

[1] H.F.Lee & W.Chen (Edits.), Advances in Microstrip and Printed Antennas (Wiley, 1997)

[2] K.S.Yee, D.Ingham and K.Shager, "Time domain extrapolation to the far fields based on FDTD calculations," *IEEE Trans. Microwave Theory Tech.*, vol. MTT 39, pp. 410-413, Mar. 1991.

[3] R.J.Luebbers, K.S.Kunz, M.Schneider & F.Hunsberger, "A finite-difference time-domain near zone to far zone transformation", IEEE Trans. Antennas Propagat., Vol.39, No.4, pp.429-435, April 1991.

[4] C. A. Balanis, *Advance Engineering Electromagnetics* (Wiley, 1989).

[5] Code *IE3D* is a product of *The Zeland Corporation*, California, USA.

[6] R.E.Horn, H.Jacobs, E.Freibergs & K.L.Kohn, "Electronic modulated beam-steerable silicon waveguide array antenna", IEEE Trans. Microwave Theory Tech., Vol.MTT-28, No.6, pp.647-653, June 1980.

[7] V.K.Varadan, V.V.Varadan, K.A.Jose & J.F.Kelly, "Electronically steerable leaky wave antenna using a tunable ferroelectric material", *Smart Materials & Structures*, Vol.3, pp.470-475, 1994.

[8] V.K.Varadan, K.A.Jose & V.V.Varadan, "Design and development of electronically tunable microstrip antennas", *Smart Materials & Structures*, Vol.8, pp.238-242, 1999.

Chapter6
General Conclusions & Future Work

The contributions of this thesis are as follows:

- We have devised a means of including independently time-varying material properties in the FDTD formulation. Although we have only applied it to the case of time-varying permittivity, it is equally applicable to cases where the permeability and conductivity are also time-varying.

- Most importantly we have systematically applied such an approach to three classes of problems, namely electromagnetic wave *propagation through* a time-varying medium, electromagnetic wave *propagation along* a time-varying medium, and electromagnetic wave *radiation from* a source on time-varying medium. The first-mentioned class of problem has received limited attention in the literature either analytically or numerically. The second and third classes have received virtually no attention in the literature using any approach.

- By carefully selecting examples from the above-mentioned classes of problem we have been able to devise means of confirming the correctness of the FDTD predictions for these examples in spite of the unavailability of precise analytical solutions (due to the inherent difficulty of finding such solutions for time-invariant problems in electromagnetics) or experimental results (due to the fact that appropriate materials are not yet extant).

- The computational analysis of the examples from the second and third class of problem, respectively the microstrip line and microstrip patch antenna on substrates with time-varying permittivity, appears to represent the first analysis of any kind to have been reported for such structures. We have shown how mixed frequencies can be generated by such structures. The geometry of these structures might be further used to emphasise or de-emphasise certain mixed frequencies.

- We have shown the effectiveness of using the FDTD method for devices comprised of time-varying substrates, and how the FDTD results can be processed (eg. using the method of determining the instantaneous frequency that was devised, or using the Fourier transform) to extract a physical understanding of the device behaviour.

We consider the work completed in this thesis to have confidently established the fact that the FDTD is a valid, and in fact perfectly suited, electromagnetic simulation method for future electromagnetic devices which might incorporate independently time-varying materials. Future work along this line might include the following:

- The application of the method to plane wave propagation through a material with a spatially-periodic pattern that moves through material over time (so-called space-time periodic media). Novel devices are currently being devised using spatially periodic structures; future use of space-time periodic media might allow even more useful features.

- The use of the tools described to study ways of realizing useful devices. This would require a detailed investigation of how existing controllable materials might be used in the manner assumed in this thesis.

APPENDIX I : MUR'S ABSORBING BOUNDARY CONDITIONS

Mur's ABCs are based on the one-way wave equation which was originally derived by Engquist and Majda [1].

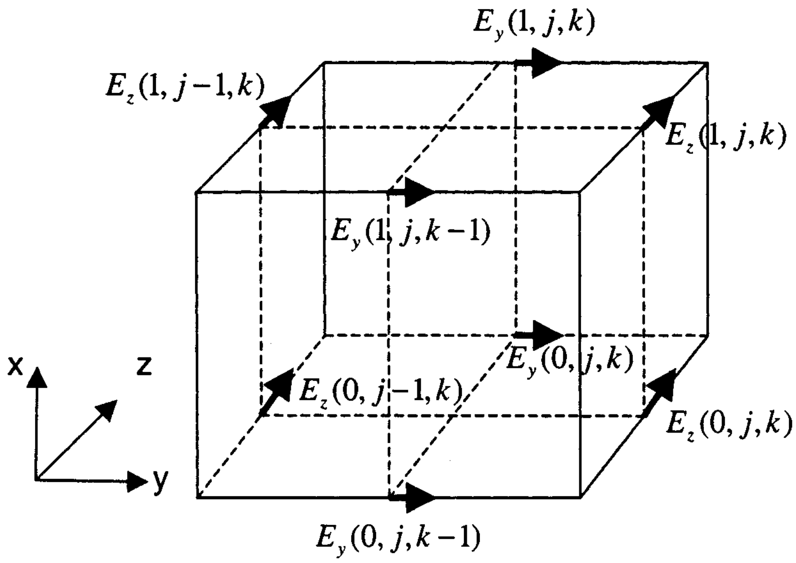

A.1 Tangential Electric Field Components on the (1,j,k) th Yee Cell at the Bottom of an FDTD Grid

The corresponding one-way wave equations for the first-order ABC are

$$(\frac{\partial}{\partial x}-\frac{1}{v}\cdot\frac{\partial}{\partial t})E_t=0 \tag{A-1}$$

To implement this equation into the FDTD algorithm, the updating equations is as [2]

$$E_t^{n+1}(0,j,k)=E_t^n(1,j,k)+\frac{v\Delta t-\Delta x}{v\Delta t+\Delta x}\cdot[E_t^{n+1}(1,j,k)-E_t^n(0,j,k)] \tag{A-2}$$

$$\begin{aligned}E_t^{n+1}(\max x,j,k)=E_t^n(\max x-1,j,k)+\frac{v\Delta t-\Delta x}{v\Delta t+\Delta x}\cdot\\ [E_t^{n+1}(\max x-1,j,k)-E_t^n(\max x,j,k)]\end{aligned} \tag{A-3}$$

$$E_t^{n+1}(i,0,k) = E_t^n(i,1,k) + \frac{v\Delta t - \Delta y}{v\Delta t + \Delta y} \cdot [E_t^{n+1}(i,1,k) - E_t^n(i,0,k)] \tag{A-4}$$

$$E_t^{n+1}(i,\max y,k) = E_t^n(i,\max y-1,k) + \frac{v\Delta t - \Delta y}{v\Delta t + \Delta y} \cdot [E_t^{n+1}(i,\max y-1,k) - E_t^n(i,\max y,k)] \tag{A-5}$$

$$E_t^{n+1}(i,j,0) = E_t^n(i,j,0) + \frac{v\Delta t - \Delta z}{v\Delta t + \Delta z} \cdot [E_t^{n+1}(i,j,1) - E_t^n(i,j,0)] \tag{A-6}$$

$$E_t^{n+1}(i,j,\max z) = E_t^n(i,j,\max z) + \frac{v\Delta t - \Delta z}{v\Delta t + \Delta z} \cdot [E_t^{n+1}(i,j,\max z-1) - E_t^n(i,j,\max z)] \tag{A-7}$$

where subscript t corresponds to the tangential components on the respective surface, i.e., $t = y, z$ on x=0 and x=$\max x$ boundaries as equations (A-2), (A-3), and $t = x, z$ on y=0 and y=$\max y$ as equations (A-4), (A-5), and $t = x, y$ on z=0 and z=$\max z$ as equations (A-6), (A-7).

For the second order ABC, the one-way equation is

$$\left(\frac{1}{v} \cdot \frac{\partial^2}{\partial x \partial t} - \left(\frac{1}{v}\right)^2 \frac{\partial^2}{\partial t^2} + \frac{1}{2}\left(\frac{\partial^2}{\partial y^2} + \frac{\partial^2}{\partial z^2}\right)\right)E_t = 0 \tag{A-8}$$

And the updating equations for the Mur's second-order ABC are as follows :

At the x=0 boundary:

$$
\begin{aligned}
E_t^{n+1}(0,j,k) = &-E_t^{n+1}(1,j,k) \\
&+\frac{v\Delta t-\Delta x}{v\Delta t+\Delta x}\cdot[E_t^{n+1}(1,j,k)+E_t^{n-1}(0,j,k)] \\
&+\frac{2\Delta x}{v\Delta t+\Delta x}\cdot[E_t^{n}(0,j,k)+E_t^{n}(1,j,k)] \\
&+\frac{\Delta x(v\Delta t)^2}{2(\Delta y)^2(v\Delta t+\Delta x)} \\
&\cdot[E_t^{n}(0,j+1,k)-2E_t^{n}(0,j,k)+E_t^{n}(0,j-1,k)+ \\
&\ [E_t^{n}(1,j+1,k)-2E_t^{n}(1,j,k)+E_t^{n}(1,j-1,k)] \\
&+\frac{\Delta x(v\Delta t)^2}{2(\Delta z)^2(v\Delta t+\Delta z)} \\
&\cdot[E_t^{n}(0,j,k+1)-2E_t^{n}(0,j,k)+E_t^{n}(0,j,k-1)+ \\
&\ [E_t^{n}(1,j,k+1)-2E_t^{n}(1,j,k)+E_t^{n}(1,j,k-1)]
\end{aligned}
\tag{A-9}
$$

At the x= max x boundary:

$$
\begin{aligned}
E_t^{n+1}(\max x,j,k) = &-E_t^{n+1}(\max x-1,j,k) \\
&+\frac{v\Delta t-\Delta x}{v\Delta t+\Delta x}\cdot[E_t^{n+1}(\max x-1,j,k)+E^{n-1}(\max x,j,k)] \\
&+\frac{2\Delta x}{v\Delta t+\Delta x}\cdot[E_t^{n}(\max x,j,k)+E_t^{n}(\max x-1,j,k)] \\
&+\frac{\Delta x(v\Delta t)^2}{2(\Delta y)^2(v\Delta t+\Delta x)} \\
&\cdot[E_t^{n}(\max x,j+1,k)-2E_t^{n}(\max x,j,k)+E_t^{n}(\max x,j-1,k)+ \\
&\ [E_t^{n}(\max x-1,j+1,k)-2E_t^{n}(\max x-1,j,k)+E_t^{n}(\max x-1,j-1,k)] \\
&+\frac{\Delta x(v\Delta t)^2}{2(\Delta z)^2(v\Delta t+\Delta z)} \\
&\cdot[E_t^{n}(\max x,j,k+1)-2E_t^{n}(\max x,j,k)+E_t^{n}(\max x,j,k-1)+ \\
&\ [E_t^{n}(\max x-1,j,k+1)-2E_t^{n}(\max x-1,j,k)+E_t^{n}(\max x-1,j,k-1)]
\end{aligned}
\tag{A-10}
$$

At the y=0 boundary :

$$
\begin{aligned}
E_t^{n+1}(i,0,k) = -E_t^{n+1}(i,1,k) \\
&+ \frac{v\Delta t - \Delta y}{v\Delta t + \Delta y}\cdot[E_t^{n+1}(i,1,k) + E_t^{n-1}(i,0,k)] \\
&+ \frac{2\Delta y}{v\Delta t + \Delta y}\cdot[E_t^{n}(i,0,k) + E_t^{n}(i,1,k)] \\
&+ \frac{\Delta y(v\Delta t)^2}{2(\Delta x)^2(v\Delta t + \Delta y)} \\
&\cdot[E_t^n(i+1,0,k) - 2E_t^n(i,0,k) + E_t^n(i-1,0,k) + \\
&[E_t^n(i+1,1,k) - 2E_t^n(i,1,k) + E_t^n(i-1,1,k)] \\
&+ \frac{\Delta y(v\Delta t)^2}{2(\Delta z)^2(v\Delta t + \Delta y)} \\
&\cdot[E_t^n(i,0,k+1) - 2E_t^n(i,0,k) + E_t^n(i,0,k-1) + \\
&[E_t^n(i,1,k+1) - 2E_t^n(i,1,k) + E_t^n(i,1,k-1)]
\end{aligned}
\tag{A-11}
$$

At the y= max y boundary :

$$
\begin{aligned}
E_t^{n+1}(i,\max y,k) = -E_t^{n+1}(i,\max y-1,k) \\
&+ \frac{v\Delta t - \Delta y}{v\Delta t + \Delta y}\cdot[E_t^{n+1}(i,\max y-1,k) + E^{n-1}(i,\max y,k)] \\
&+ \frac{2\Delta y}{v\Delta t + \Delta y}\cdot[E_t^{n}(i,\max y,k) + E_t^{n}(i,\max y-1,k)] \\
&+ \frac{\Delta y(v\Delta t)^2}{2(\Delta x)^2(v\Delta t + \Delta y)} \\
&\cdot[E_t^n(i+1,\max y,k) - 2E_t^n(i,\max y,k) + E_t^n(i-1,\max y,k) + \\
&[E_t^n(i+1,\max y-1,k) - 2E_t^n(i,\max y-1,k) + E_t^n(i-1,\max y-1,k)] \\
&+ \frac{\Delta y(v\Delta t)^2}{2(\Delta z)^2(v\Delta t + \Delta y)} \\
&\cdot[E_t^n(i,\max y,k+1) - 2E_t^n(i,\max y,k) + E_t^n(i,\max y,k-1) + \\
&[E_t^n(i,\max y-1,k+1) - 2E_t^n(i,\max y-1,k) + E_t^n(i,\max y-1,k-1)]
\end{aligned}
\tag{A-12}
$$

At the z=0 boundary :

$$
\begin{aligned}
E_t^{n+1}(i,j,0) = -E_t^{n+1}(i,j,1) \\
&+\frac{v\Delta t-\Delta z}{v\Delta t+\Delta z}\cdot[E_t^{n+1}(i,j,1)+E_t^{n-1}(i,j,0)] \\
&+\frac{2\Delta z}{v\Delta t+\Delta z}\cdot[E_t^{n}(i,j,0)+E_t^{n}(i,j,0)] \\
&+\frac{\Delta z(v\Delta t)^2}{2(\Delta x)^2(v\Delta t+\Delta z)} \\
&\cdot[E_t^{n}(i+1,j,0)-2E_t^{n}(i,j,0)+E_t^{n}(i-1,j,0)+ \\
&\;[E_t^{n}(i+1,j,1)-2E_t^{n}(i,j,1)+E_t^{n}(i-1,j,1)] \\
&+\frac{\Delta z(v\Delta t)^2}{2(\Delta y)^2(v\Delta t+\Delta z)} \\
&\cdot[E_t^{n}(i,j+1,0)-2E_t^{n}(i,j,0)+E_t^{n}(i,j-1,0)+ \\
&\;[E_t^{n}(i,j+1,1)-2E_t^{n}(i,j,1)+E_t^{n}(i,j-1,1)]
\end{aligned}
\tag{A-13}
$$

At the z= $\max z$ boundary :

$$
\begin{aligned}
E_t^{n+1}(i,j,\max z) = -E_t^{n+1}(i,j,\max z-1) \\
&+\frac{v\Delta t-\Delta z}{v\Delta t+\Delta z}\cdot[E_t^{n+1}(i,j,\max z-1)+E_t^{n-1}(i,j,\max z)] \\
&+\frac{2\Delta z}{v\Delta t+\Delta z}\cdot[E_t^{n}(i,j,\max z)+E_t^{n}(i,j,\max z-1)] \\
&+\frac{\Delta z(v\Delta t)^2}{2(\Delta x)^2(v\Delta t+\Delta z)} \\
&\cdot[E_t^{n}(i+1,j,\max z)-2E_t^{n}(i,j,\max z)+E_t^{n}(i-1,j,\max z)+ \\
&\;[E_t^{n}(i+1,j,\max z-1)-2E_t^{n}(i,j,\max z-1)+E_t^{n}(i-1,j,\max z-1)] \\
&+\frac{\Delta z(v\Delta t)^2}{2(\Delta y)^2(v\Delta t+\Delta z)} \\
&\cdot[E_t^{n}(i,j+1,\max z)-2E_t^{n}(i,j,\max z)+E_t^{n}(i,j-1,\max z)+ \\
&\;[E_t^{n}(i,j+1,\max z-1)-2E_t^{n}(i,j,\max z-1)+E_t^{n}(i,j-1,\max z-1)]
\end{aligned}
\tag{A-14}
$$